

MIT Open Access Articles

Effect of temperature on ion transport in nanofiltration membranes: Diffusion, convection and electromigration

The MIT Faculty has made this article openly available. **Please share** how this access benefits you. Your story matters.

Citation: Roy, Yagnaseni et al. "Effect of Temperature on Ion Transport in Nanofiltration Membranes: Diffusion, Convection and Electromigration." *Desalination* 420 (October 2017): 241–257 © 2017 Elsevier B.V.

As Published: <http://dx.doi.org/10.1016/j.desal.2017.07.020>

Publisher: Elsevier

Persistent URL: <http://hdl.handle.net/1721.1/110933>

Version: Author's final manuscript: final author's manuscript post peer review, without publisher's formatting or copy editing

Terms of use: Creative Commons Attribution-Noncommercial-Share Alike



Journal paper citation: Effect of temperature on ion transport in nanofiltration membranes: Diffusion, convection and electromigration, Yagnaseni Roy, David M. Warsinger, John H. Lienhard V, Desalination 420C (2017) pp. 241-257

Effect of temperature on ion transport in nanofiltration membranes: Diffusion, convection and electromigration

Yagnaseni Roy¹, David M. Warsinger¹, John H. Lienhard V^{*, 1}

¹ Department of Mechanical Engineering, Massachusetts Institute of Technology, Cambridge, MA 02139-4307, USA

Abstract

Nanofiltration performance as a function of feed temperature is relevant to several industrial settings including pretreatment for scale control in thermal desalination. Understanding of solute transport as a function of temperature is critical for effective membrane and system design. In this study, nanofiltration is modeled at 22, 40 and 50°C using the Donnan Steric Pore Model with dielectric exclusion (DSPM-DE). This modeling includes the temperature dependence of the three modes of solute transport, namely the convective, electromigrative, and diffusive modes, and the three mechanisms of solute exclusion, namely Donnan, steric, and dielectric exclusion. The effect of temperature is captured through the variation of membrane parameters and solvent and ionic mobilities with temperature. We compare the most abundant ionic compound in natural water, sodium-chloride with magnesium-chloride to portray how the salt passage and rejection change for a 1:1 salt compared to a 2:1 salt, and we analyze Arabian Gulf seawater to understand how rejection of scale-forming ions, such as Mg^{2+} and Ca^{2+} , is affected by feed temperature. In all cases, solute transport increases with temperature, attributed predominantly to the cumulative effect of membrane parameters and only to a small extent (up to 5%) to the solvent viscosity and ion diffusivity together.

Keywords: Nanofiltration, Temperature, Ion transport, Desalination

* Corresponding author: Email address: lienhard@mit.edu; Tel. +1 617-253-1000

Graphical abstract

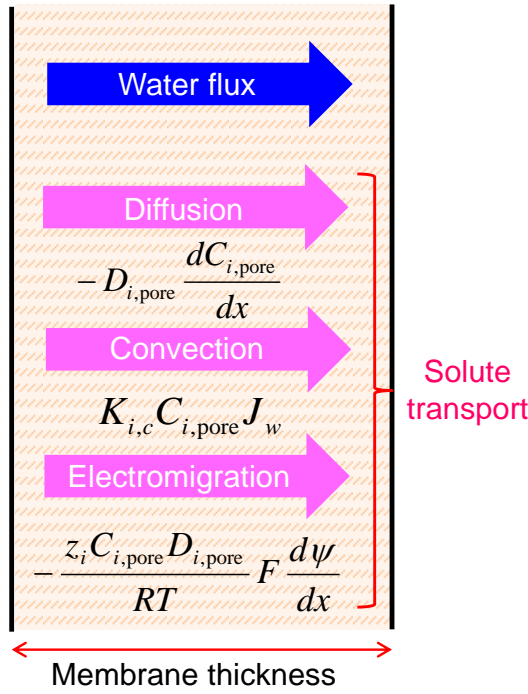
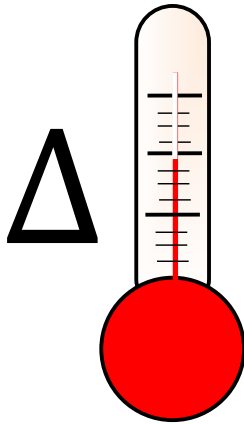
Change in feed temperature



alters transport in nanofiltration



affecting rejection differently for varying feed solutions



NaCl
MgCl₂
Seawater ?

Nomenclature

A_k	porosity of membrane	
C	concentration	mol m^{-3}
C_x	membrane volumetric charge density	mol m^{-3}
d	thickness of a single water molecule (0.28 nm)	nm
D	solute diffusivity	$\text{m}^2 \text{s}^{-1}$
F	Faraday's constant	C eq^{-1}
j	solute flux	$\text{mol m}^{-2}\text{s}^{-1}$
J_w	solvent permeation flux	m s^{-1}
K_c	hindrance factor for convection	
K_d	hindrance factor for diffusion	
N_c	number of components in the mixture	
r_{pore}	pore radius of membrane	m
R	universal gas constant	$\text{J mol}^{-1} \text{K}^{-1}$
T	temperature	K
x	distance normal to membrane	m
Δx	membrane active layer thickness	m
z	valence of species	

Greek symbols

ε	dielectric constant of medium	
ε^*	dielectric constant of oriented water layer inside pores	
λ	ratio of solute Stokes radius to pore radius	
ν	kinematic viscosity	$\text{m}^2 \text{s}^{-1}$
ρ	density	kg m^{-3}
Φ_i	steric partitioning factor	
Φ_B	Born solvation factor for partitioning	
ψ	membrane potential	V

Subscripts

D	Donnan potential
i	solute species
m	feed-membrane interface
p	permeate just outside the membrane
$pore$	inside pore
w	solvent
∞	bulk

Dimensionless Parameters

$R_{C/E}$	ratio between the convective and electromigrative terms
$R_{E/D}$	ratio between the electromigrative and diffusive terms

1. Introduction

1.1. Significance of nanofiltration for elevated feed temperatures

In a world where water-scarcity is a burgeoning issue, methods of water-treatment and reuse that are economic and minimize energy consumption are of vital importance for the safekeeping of the environment [1]. Nanofiltration (NF) is a pressure driven membrane-based desalination technique. The pore sizes of NF membranes are between that of reverse osmosis (RO) and ultrafiltration (UF) membranes [2] [3] [4] [5] [6] . NF has the unique capability to preferentially remove multivalent ions [7] [8]. In several applications, water temperature varies from point-to-point in the treatment plant or changes over time [9]. For example, NF-MSF (nanofiltration with multistage flash) and NF-MSF-RO (nanofiltration with multistage flash and reverse osmosis), are widely studied applications of NF in hybrid with thermal desalination systems where feed (seawater or brackish water) temperature changes over the year and the performance of the nanofiltration membrane changes noticeably with temperature [10]. Nanofiltration also has other high temperature applications: in the textile industry, water used for bleaching and dyeing may reach temperatures up to 90°C; in the pulp and paper industry, the water temperature is often above 60°C [11]. Water temperature is usually reduced before membrane treatment. This practice requires expenditure on heat exchangers and also creates energy costs due to the inefficiencies of the heat exchangers [12]. Thus, by designing NF membranes for optimal performance at above ambient temperature, capital costs and energy consumption in heat-exchangers, dependence on other energy-intensive water-treatment methods such as RO, and the use of chemical additives to remove scale-forming ions can be reduced significantly [13]. Detailed modeling of nanofiltration (NF) with variation in feed temperature is necessary to achieve this, as the rejection of undesired components can vary significantly as a result of changing temperature.

1.2. The DSPM-DE model of nanofiltration

This work uses the Donnan Steric Pore Model with Dielectric Exclusion (DSPM-DE) to analyze the temperature dependence of nanofiltration. This model has been used widely into recent times to model

and explain nanofiltration performance using a variety of feed solutions with success [14] [15] [16] [17] [18] [19]. DSPM-DE is a comprehensive model for nanofiltration. As the name suggests, the model provides information regarding the magnitudes of the different modes of solute exclusion occurring at the membrane-solution interfaces, namely steric exclusion (size-based exclusion at the pore opening), Donnan effect (repulsion or attraction effect due to membrane potential) and dielectric exclusion (resistance to the solute entering the membrane pores due to an energy barrier associated with shedding of the solute hydration shell in order to enter the pore) [20] [21] [22]. The model uses the Nernst-Planck equation to describe solute transport through the membrane and hence provides information on the individual modes of transport within the membrane, namely diffusion (movement of solute down a concentration gradient), convection (solute transported by bulk fluid motion) and electro-migration (ion movement due to the membrane potential gradient). As inputs to this model, the membrane is characterized by certain structural parameters (pore radius and effective active layer thickness) and electrical parameters (membrane charge and pore dielectric constant) [21] [23]. These nanofiltration membrane properties are affected by experimental conditions such as feed composition, pH, concentration and temperature [24] [25] [10]. An understanding of how membrane properties affect the modes of solute exclusion and solute transport for different solutes is important in order to gain intuition about nanofiltration. Such understanding will ultimately allow one to gain intuition of how experimental conditions such as temperature affect rejection and solvent flux characteristics of nanofiltration membranes.

1.3. Conventional understanding of the effect of temperature on nanofiltration

Usually, water flux through nanofiltration membranes increases with increase in temperature, while uncharged solute rejection reduces with increase in temperature and the variation of charged solute rejection with temperature depends on the ion and the membrane used. Although experimental evidence for these observations is abundant in literature, the understanding of how the membrane itself changes and related modeling work is missing in literature. For instance, from the study of Manttari et al. [11] on the

nanofiltration of glucose and pulp mill effluent over a temperature range of 25°C to 65°C using several different membranes, the authors found that the rejection of uncharged solutes decreased by ~20% from 20°C to 55°C and the overall rejection of the ionic species remained almost unchanged (at ~90%) over the same range of temperature. Schaep et al. [26] experimentally studied the nanofiltration of ground water using the UTC-20 NF membrane over a temperature range of 10°C to 30°C and found that water flux at 30°C is 1.5 times that at 10°C. In their study, the rejection of monovalent ions (sodium, chloride and potassium) decreased significantly over the given range of temperature, while the rejection of divalent ions (calcium, magnesium and sulfate) was barely affected by temperature, showing only a slight increase with increase in temperature [26]. In another study by Nilsson et al. [27], the Alfa Laval NFT-50 nanofiltration membrane was used over a temperature range of 20°C-50°C keeping solvent flux constant, and the results showed that the rejection ratio of potassium-chloride decreased less noticeably than that of glucose. While Schaep et al. [26] interpret the observed changes in ion passage with temperature based on the increase in solute diffusivity with temperature, Nilsson et al. [27] justify their observations based on membrane charge effects.

Although there is abundant literature on nanofiltration of charged solutes at different temperatures, to the best of the authors' knowledge, none of them attempt to fit parameters as a function of temperature with respect to the DSPM-DE model, taking into consideration change in membrane charge and pore dielectric constant. Nilsson et al. [27] mention that there is no significant change in the isoelectric point of the Alfa Laval NFT-50 membrane with variation of temperature, hence indicating that the membrane charge properties are not greatly affected by temperature. However, it is unclear whether this is a general trend for all membranes without the relevant data from other membranes. Furthermore, as seen in the work of Schaep et al. [26], the rejection ratio of certain ions shows dramatic change with temperature, and it is questionable whether that is simply a result of a change in ion diffusivity as a function of temperature, as mentioned by the authors, or of changes in membrane charge and pore dielectric constant also.

Knowledge of the extent to which each of the quantities (solvent viscosity, solute diffusivity, membrane structural and electrical parameters) are affected by temperature and the resulting effect they have on ion passage would allow one to explain the experimental results with certainty. The work of Amar et al. [10] concludes that it is not sufficient to consider only the change in solvent viscosity and solute diffusivity in order to explain the increased water flux and reduced rejection of uncharged solutes with increase in temperature and that the change in membrane structural parameters with temperature are essential to correctly explain how nanofiltration of uncharged solutes is affected by temperature. However, their work is restricted by its applicability to only uncharged solutes.

1.4. Aims of this study

In this work, the effect of temperature on nanofiltration membrane properties and the resulting effect on ion and solvent transport through the membrane are studied, using three different feed compositions. The DSPM-DE model is used to model nanofiltration of charged solutes at different temperatures. The objective is to not only observe the resulting change in membrane performance but to gain intuition on how ions of different valence, size and diffusivity are affected differently by temperature.

2. Governing Equations

2.1. Historical development of the DSPM-DE model

As mentioned earlier, the model used for this study is the Donnan Steric Pore Model with dielectric exclusion (DSPM-DE). Despite its complexity, the model's thoroughness has made it become widely used for modeling nanofiltration, and it has been used successfully in the literature to model experimental membrane performance [21] [25] [28]. This model evolved from the hindered transport theory of uncharged solutes in pores introduced by Anderson et al. in 1974 [29] [30], which was later extended for ionic species by including the electrochemical potential gradient in the solute transport equation, leading to electrokinetic models that use the extended Nernst-Planck equation (e.g. the Space-charge model and TMS models) [31] [32]. One such model was the DSPM (Donnan-Steric Pore Model) introduced by

Bowen et al. [23] in the late 1990s and it was the precursor of the DSPM-DE model. The DSPM considered only the steric and Donnan exclusion mechanisms. This model quickly became popular and was successful in modeling nanofiltration of a wide variety of solutions, even those consisting of multivalent co-ions (ions with the same charge as the membrane) [20] [22] [33]. However, its major drawback was in its failure to model experiments with multivalent counter-ions. This failure was attributed to the deficiency of the exclusion mechanisms considered. The DSPM-DE model includes an additional exclusion mechanism, known as dielectric exclusion which allowed researchers to overcome the difficulties in modeling multivalent counter-ions [20].

However, the concept of dielectric exclusion and the mechanism by which it works has been widely debated over the years. Some authors suggest that the Donnan exclusion mechanism is sufficient to explain rejection of ions, including counter-ions. For example, Higa et al. [34] showed that a solution with Ca^{2+} , K^+ and Cl^- ions passing through a negatively charged membrane can be modeled successfully by considering only Donnan exclusion. Other authors have found Donnan exclusion to be insufficient in modeling nanofiltration, as mentioned previously while discussing the transition of the DSPM to DSPM-DE. Evidence from molecular dynamics simulation of membranes with nanopores, however, describes dielectric exclusion as an undeniable phenomenon [35] [36]. Yaroshchuk et al. [37] further mention that the dielectric exclusion is a ‘universal phenomenon’ and should be considered alongside steric and Donnan exclusion. Bandini et al. [22] mention two mechanisms for dielectric exclusion by nanofiltration membranes: image forces and the Born effect. However according to Bowen et al. [21], in nanofiltration, the Born effect of dielectric exclusion is more dominant than the effect of image charges that develop at the interface of the membrane and bulk solution. This is because the small pores in nanofiltration membranes cause the intra-pore dielectric constant of the solvent to be almost equal to that of the membrane material itself. Furthermore, the image charges are screened by electric double layers in electrolyte solutions [21]. The DSPM-DE model in the form introduced by Bowen and Welfoot [21] has been used successfully by several authors, including in recent years for a variety of feed compositions

[16] [18] [19]. In reference [21], Bowen and Welfoot successfully implemented the DSPM-DE model for the same membrane considered in the current work (Desal5DK) accounting for only the Born mechanism of dielectric exclusion for sodium-chloride and magnesium-chloride. In their study, they also showed experimental results over the same range of feed concentration considered in the current work, which justifies the use of this model for the simulations here.

In the current work the DSPM-DE model equations are implemented using MATLAB vR2015b following the approach by Geraldes et al. [20], in which only the Born effect on dielectric exclusion is incorporated [20] (as per the formulation in [21]). This effect is described in detail in section 4.4. The DSPM-DE model in this form has been well validated with lab-scale experiments [20] [25]. In this model, the membrane is characterized by structural parameters (effective pore radius and active layer thickness) and electrical parameters (membrane charge and pore dielectric constant). The inclusion of the dielectric exclusion mechanism in addition to Donnan exclusion and steric exclusion for the current study allows the work to be broad and include all important effects determining solute transport through a nanofiltration membrane with temperature change.

2.2. Governing equation for solute flux

The solute flux through the membrane is governed by the Extended Nernst-Planck equation (ENP). For each solute '*i*', the ENP equation is given by Eq. (1) [14] [20].

$$j_{i,pore} = -D_{i,pore} \frac{dC_{i,pore}}{dx} - \frac{z_i C_{i,pore} D_{i,pore}}{RT} F \frac{d\psi}{dx} + K_{i,c} C_{i,pore} J_w \quad (1)$$

where $j_{i,pore}$ is the solute flux of the species '*i*', consisting of the diffusive, electromigrative and convective terms respectively, in the order they appear in the equation. $D_{i,pore}$, $C_{i,pore}$ and z_i are the intra-pore diffusion coefficient, concentration and valence respectively of species *i*, J_w is the water flux through the membrane, ψ is the membrane potential. Due to the extremely small pore sizes in

nanofiltration membranes, the ‘hindered transport theory’ is used and thus the terms of the ENP are modified by hindrance factors $K_{i,c}$ (for the convective term) and $K_{i,d}$ (that multiplies the bulk diffusivity) to give the diffusivity in the pore, as found in the diffusive and electromigrative terms. Thus $D_{i,pore} = K_{i,d}D_{i,\infty}$. Both these factors are functions of the ratio of the solute radius to pore radius, λ_i [20], [21], [14], [30], [38]. The model treats the pores as perfectly cylindrical and the solutes as perfect hard spheres [39] [40] [41]. Figure 1 schematically describes each of the modes of solute transport considered in the Extended Nernst-Planck equation. The diffusive term exists due to the concentration gradient of each species within the membrane, while the convective term is the transport of the solute as a result of ‘being carried’ by the solvent through membrane pores. The electromigrative term is a result of the gradient of membrane potential through the membrane. The membrane potential is an electrostatic potential that develops to balance ionic fluxes and maintain quasi-electroneutrality within the membrane [20].

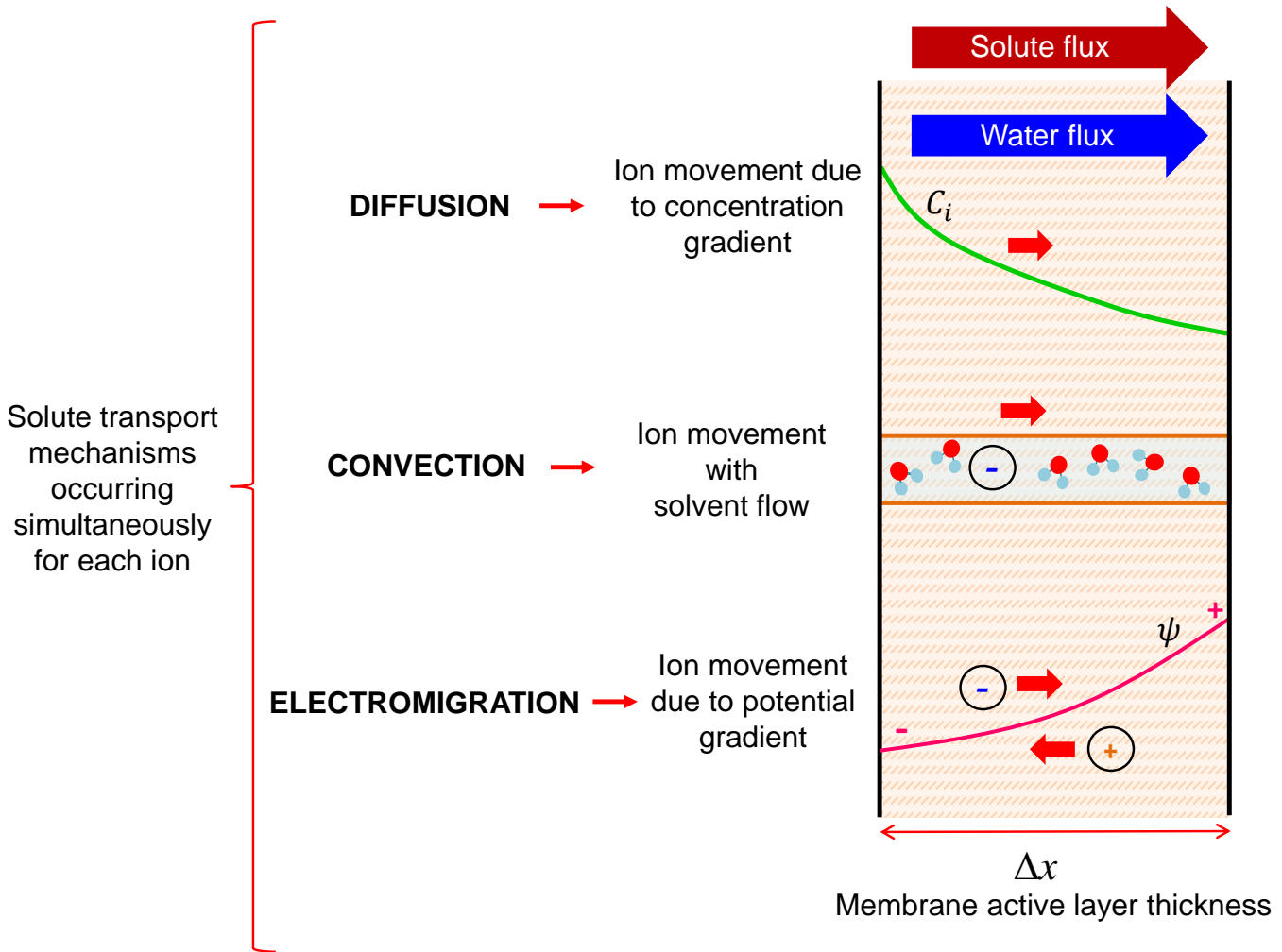


Figure 1. Schematic representation of solute transport mechanisms in the current model described by the Extended Nernst-Planck (ENP) equation, which is a component of the Donnan Steric Pore model with Dielectric Exclusion (DSPM-DE).

2.3. Equilibrium boundary conditions on membrane-solution interfaces due to solute exclusion mechanisms

At the membrane-feed solution interface, the equilibrium boundary condition is established due to the combination of the three exclusion mechanisms considered in the DSPM-DE model: the steric exclusion, dielectric exclusion (due to the Born effect, which accounts for the solvation energy barrier for the ion to

enter the pore, cf. section 4.4.) and Donnan exclusion. These mechanisms are represented schematically in Fig. 2.

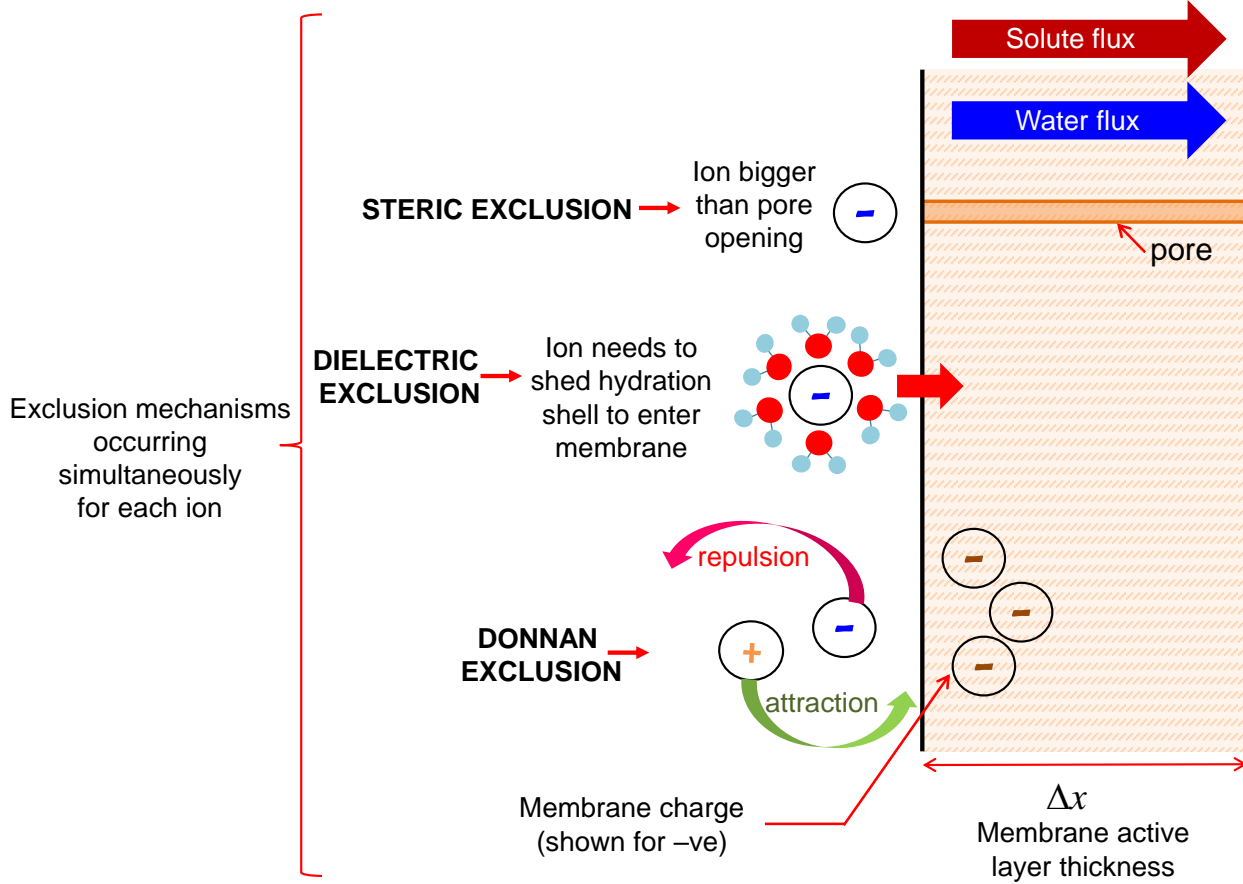


Figure 2. Schematic representation of solute exclusion mechanisms in nanofiltration as per the Donnan Steric Pore Model with Dielectric Exclusion (DSPM-DE).

Mathematically, these effects are described by Eq. 2 ([14], [20]):

$$\frac{\gamma_{i,pore} c_{i,pore}}{\gamma_{i,m} c_{i,m}} = \Phi_i \Phi_B \exp\left(-\frac{z_i F}{RT} \psi_{D,m}\right) \Big|_{in} \quad (2)$$

where $C_{i,pore}$ is the solute concentration just within the pore 'entrance'; $C_{i,m}$ is the feed concentration at the membrane-feed solution interface; and $\gamma_{i,m}$, $\gamma_{i,pore}$, are solute i 's activity coefficients at the membrane-feed solution interface and just within the pore entrance respectively (calculated by the Davies

equation [14] [20]). Φ_i, Φ_B are the steric partitioning factor and Born solvation partitioning factor, respectively, which represent the extent of exclusion experienced by the ion due to these effects. These two partitioning factors are numbers smaller than unity such that a smaller value indicates higher exclusion. The effect of the partitioning factors is evident from the left hand side of Eq. 2, which indicates that a smaller value of Φ_i or Φ_B causes a reduction of the ratio between solute concentration within the membrane pore ($C_{i,pore}$) to the concentration immediately outside the membrane ($C_{i,m}$, due to concentration polarization). The term $\psi_{D,m}$ is the Donnan potential on the feed side, defined as the potential difference between the point just within the pore entrance and the solution (at the feed-membrane interface) [20]. The expressions for the steric partitioning factor, the Born solvation partitioning factor and the two hindrance factors are given in [14] and used in the present model.

Similarly, the boundary condition on the permeate side (i.e. at the membrane-permeate interface) is given by [14] [20]:

$$\frac{\gamma_{i,pore} C_{i,pore}}{\gamma_{i,p} C_{i,p}} = \Phi_i \Phi_B \exp\left(-\frac{z_i F}{RT} \psi_{D,p}\right) \Big|_{out} \quad (3)$$

where $C_{i,pore}$ is now the concentration at the pore exit (just within the membrane) and $C_{i,p}$ is the permeate concentration, just outside the membrane; $\psi_{D,p}$ is the Donnan potential difference between these two points.

Equations (2) and (3) state that the ratio of concentrations just within the membrane and that at the membrane-feed/permeate solution is governed by the steric, dielectric and Donnan exclusion effects. Figure 2 schematically explains each of the exclusion mechanisms considered in the DSPM-DE model.

2.4. Electroneutrality conditions

Within each domain considered in the model, i.e. the bulk feed solution, the concentration polarization boundary layer (membrane-feed interface), the membrane, and the permeate solution, there can be no net

charge (the electroneutrality condition) [20]. Within the membrane, the electroneutrality condition is described as:

$$\sum_{i=1}^{N_c} z_i C_{i,pore} = -C_X \quad (4)$$

where N_c is the number of species/components in the mixture, z_i is the valence of the species i and C_X is the volumetric charge density of the membrane. Similar electroneutrality equations can be written for the bulk feed, membrane-feed interface and permeate by using the relevant concentration and setting the volumetric charge density to zero, since no net charge is present at any point outside the membrane [20].

2.5. Solvent flux

As described by Bowen et al. [21] and Wang et al. [14], the flow of water through the membrane has been successfully modeled by a creeping laminar flow in the form of the Hagen-Poiseuille equation. Therefore, the transmembrane solvent flux J_w as a function of membrane structural parameters and net driving pressure is given by [14]:

$$J_w = \Delta P_{net} \left(\frac{r_{pore}^2}{8\nu\rho_w \left(\frac{\Delta x}{A_k} \right)} \right) \quad (5)$$

where r_{pore} is the membrane pore radius and $\Delta x/A_k$ is the effective active layer thickness, taking into account membrane porosity A_k . The fluid properties used in the expression are ν , the kinematic viscosity of the solvent and ρ_w , the density of the solvent. ΔP_{net} is the net pressure across the membrane, which is the hydraulic pressure applied, minus the osmotic pressure difference across the membrane [14].

Figure 3 illustrates how the exclusion mechanisms come together to influence the concentration profile across the membrane. A nanofiltration membrane with either positive or negative membrane volumetric charge density is shown. The feed side is pressurized so that water flux and solute flux both go from the

feed to the permeate side. Cross-flow velocity over the membrane is assumed to be high enough so that no concentration polarization occurs. Concentration jumps from the feed value to that within the membrane on the feed side due to the feed side partitioning effect (cf. Eq. 2). A similar effect is seen on the permeate side (cf. Eq. 3). The partitioning results from a combination of the steric, dielectric and Donnan exclusion effects, as mentioned earlier. The ion with charge opposite to that of the membrane (membrane counter-ion) is in greater abundance inside the membrane, as shown by the green concentration profile, whereas the membrane co-ion is less abundant and is represented by the blue concentration profile. The concentration profiles shown in this diagram represent only the simple case of a binary 1:1 salt, i.e. a salt with one cation and one anion of equal and opposite valence. Thus, in order to maintain electroneutrality, the concentrations of both ions at any point outside the membrane have to be equal to each other whereas within the membrane, the electroneutrality condition is satisfied by including the membrane charge density (cf. Eq. 4), thereby resulting in membrane counter-ion concentration to be larger than that of the co-ion inside the membrane. In most cases described subsequently, the rejection ratio is positive and the permeate concentration is less than that of the feed side.

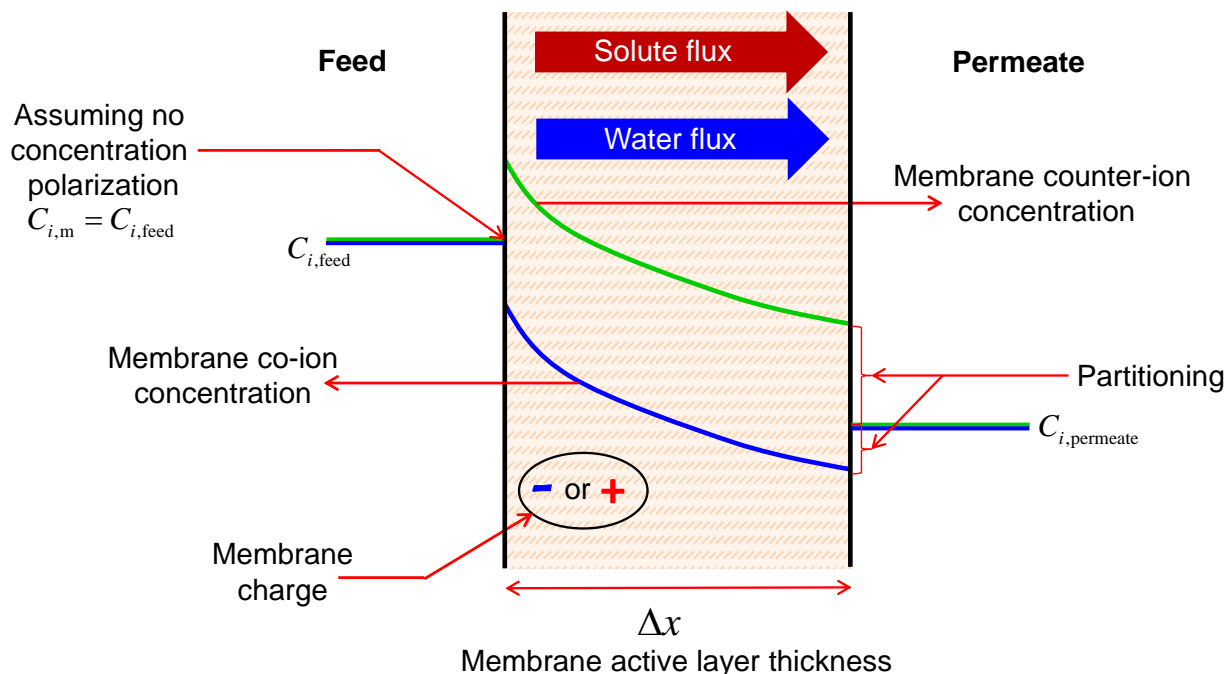


Figure 3. Concentration profiles of ions from a binary 1:1 salt through the membrane thickness in a nanofiltration membrane

3. Validation

In this study, the membrane structural parameter values at different temperatures are taken from experimental work by Amar et al. [10] (cf. Appendix A). Those authors fit membrane pore radius and effective active layer thickness of the Desal5DK membrane at different temperatures using the hindered transport theory, assuming the solute particles are hard spheres travelling through cylindrical pores. They obtain the effective pore size for the membrane at each temperature by taking the average fitted value from a number of uncharged solutes at those temperatures in the limit of high Péclet number where the rejection versus solvent flux plot plateaus. They provide the effective membrane thickness individually for each solute. Their work assumes that no concentration polarization occurs in the system. As mentioned previously, the model used for the present study is also based on the hindered transport theory, and so the fitting parameters obtained by Amar et al. [10] are expected to work well in the present work.

Figure 4 shows the experimental data from Amar et al. [10] along with results from the current model for arabinose, at the three temperatures to be considered in this study, 22°C, 40°C and 50°C. In the model used for this work, equations 1-3 described above are discretized as shown in [20] and solved numerically using MATLAB (version R2015b). The difference between the experimental data and the modeling results are below 5% in most cases, except for the two data points at the lowest values of solvent flux at 40°C and 50°C. This is, however, in accordance to the modeling by Amar et al. [10] as can be seen in Fig. 12 in their paper, which shows the comparison between experimental data and their modeling when changes in all four modeling components required for uncharged solutes (two membrane structural parameters, solvent viscosity and solute diffusivity) with temperature are taken into account. The better agreement between modeling and experiment at higher values of water flux (and correspondingly higher Péclet number) both in the work of Amar et al. [10] and in this work is not surprising given that the fitting was done in the range of high Péclet number, as mentioned earlier. It is common practice to use membrane structural parameters obtained from fitting with respect to uncharged solute data for modeling solutions containing charged solutes. Membrane charge and pore dielectric constant are then fitted in order to model nanofiltration of charged solutes accurately [24] [25] [28].

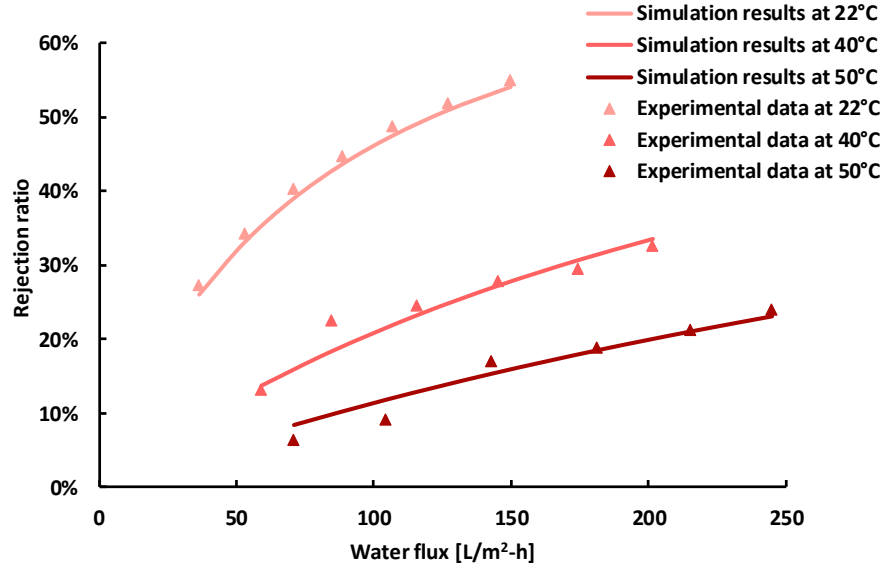


Figure 4. Validation of current DSPM-DE modeling with experimental NF data of Amar et al. [10]

The objective of this paper is to explain the changes in ion transport through the Desal5DK membrane at different temperatures by taking into account the temperature dependence of all four membrane parameters as well as the change in solvent viscosity and solute diffusivity. Since the exact change of membrane charge for the Desal5DK membrane with respect to temperature is not currently known, a parametric study will be done with respect to this quantity, hence providing insight into a wide range of possible cases. An analytical expression for the pore dielectric constant, described in detail in a later section, will be used to estimate this quantity as a function of temperature.

4. Results and Discussion

In this section, solute transport mechanisms for sodium-chloride, magnesium-chloride and seawater ions at different temperatures are analyzed. Results are presented and discussed for 3 temperatures (22°C, 40°C and 50°C) for conciseness and simplicity. In the supplementary information section, results for 30°C in addition to the 3 temperatures described here are presented to show that the trends with temperature described in the current paper hold through the entire temperature range from 22-50°C.

4.1. Property variation at higher temperature

The principal new methodology applied in this work is the use of the DSPM-DE to conditions with increasing temperature. At higher temperature, numerous input variables for the model change. A summary of these parameters is given in table 1. To the best of the current authors' knowledge, this work is the first to consider the variation of these properties to the DPM-DE model for NF. The membrane structural parameters (r_{pore} and $\Delta x/A_k$) vary with temperature due to the restructuring of the polymer material. The variation of the pore dielectric constant with temperature is described further in section 4.4.1. and is due to the combined effect of membrane pore size variation and variation of solvent dielectric constant with temperature.

Table 1. Input variables to the DSPM-DE model that vary by temperature

Symbol	Variable	Units	Source	Change at higher temperature
ν	Solvent kinematic viscosity	$m^2 s^{-1}$	Ref [42]	Decreases
r_{pore}	Pore radius	m	[10], Table 4	Increases
$\Delta x/A_k$	Effective membrane thickness (for both solute and water)	m	[10], Table 4, Fig 17.	Varies
D_i	Solute Diffusivity	$m^2 s^{-1}$	Stokes-Einstein Eq., [27]	Increases
\mathcal{E}_{pore}	Pore dielectric constant	-	Eq. 9	Increases

4.2. Sodium-chloride (NaCl) transport as a function of temperature

In this section, the transport of sodium and chloride ions through the membrane is analyzed at different temperatures. Sodium-chloride is the dominant salt by mass in most waters considered for desalination, and often a desirable property of NF membranes is sodium-chloride passage with exclusion of other salts that have scaling potential. The effect of temperature is captured in the change of the structural parameters of the membrane as obtained from Amar et al. [10] as well as the change in ion diffusivity and

solvent viscosity. In addition, the effect of membrane charge on the ion transport and rejection is observed. A subsequent section will discuss the effect of dielectric exclusion in detail. In addition to the net solute transport, the convective, diffusive and electromigrative fluxes are also observed individually. Since correlations for membrane parameter variation (both structural and electrical) with temperature are not available in literature, the simulation results are shown here at just the few temperatures for which structural parameters are given by Amar et al. [10]. The range of temperature studied by Amar et al. [10] (22-50°C) is practically relevant because the lower limit represents the temperature at which several lab-scale experiments are conducted ([21], [24]) and at which membrane specifications from the manufacturer are provided. The upper limit of 50°C is slightly lower than the upper limit of the temperature tolerance of the experimental setup used in reference [10] and represents the typical temperature of geothermal brackish water which is often used as NF feed [10].

For the results that follow, the feed concentration of sodium-chloride is 0.01 M for all cases. Concentration polarization is neglected, assuming a high cross-flow over the membrane with associated high mass transfer coefficients. Although concentration polarization may not be negligible in some common industrial applications, small lab setups can reach this condition. This approach allows us to ignore the flow properties on either side of the membrane in developing the results for membrane performance.

4.2.1. Net solute transport change with temperature

The model shows that the solvent transport and net solute transport always increase as temperature is increased. As a result, the rejection ratio always decreases with increasing temperature as seen in Fig. 5a. Furthermore, it is seen that each of the convective, diffusive and electromigrative contributions to solute flux increase in absolute value with temperature as well. These effects occur as a result of the change in membrane structural parameters, solvent viscosity and solute diffusivity due to temperature at each value of membrane charge.

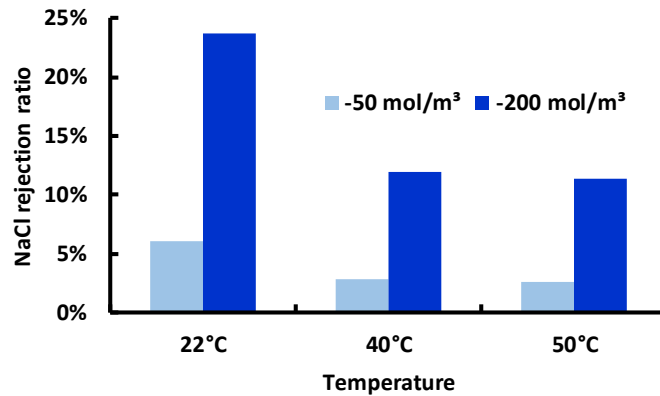


Fig. 5a. NaCl rejection ratio vs. T

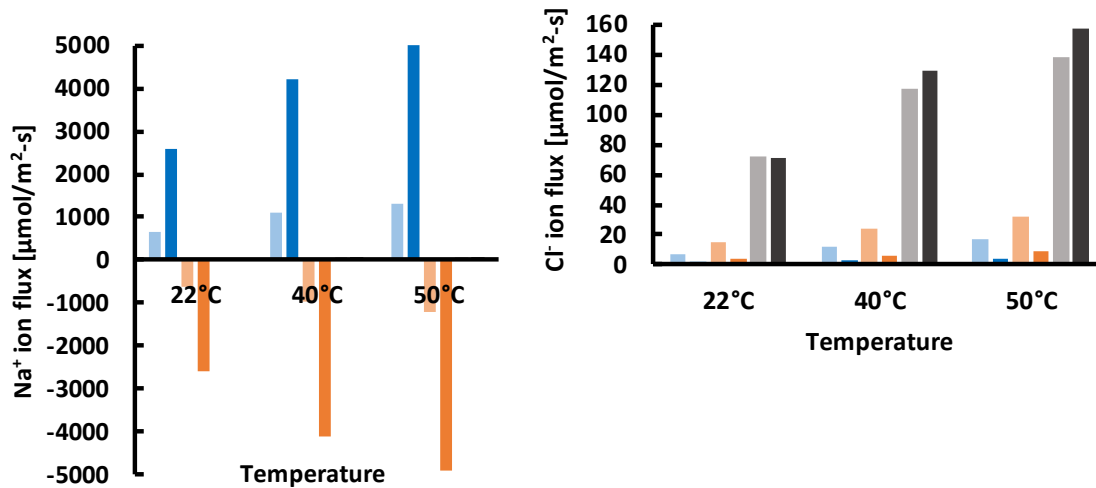


Fig. 5b. Na⁺ flux vs. T

Fig. 5c. Cl⁻ flux vs. T



Figure 5. For a negatively charged NF membrane (-50 or -200 mol m^{-3}), modeling results for rejection and solute transport of Na^+ and Cl^- ions in a $0.01M$ NaCl solution at different temperatures: (a) rejection of NaCl; (b) transport of Na^+ ions by the three modes; and (c) transport of Cl^- ions by the three modes.

4.2.2. Change in solution and membrane properties with temperature

Some of the temperature-dependent properties mentioned in section 4.1. were more dominant in influencing solute flux (and hence rejection) and solvent flux through the membrane with temperature variation than others. As temperature increased, changes in the membrane structural parameters (i.e., pore radius and membrane thickness) together had a much more prominent influence on membrane

performance than the solvent and solute mobilities combined. The effects of these two sets of parameters can be separated by running the simulation in two steps. At first, all effects are considered to vary with temperature together. Subsequently, the effect of increased solute and solvent mobilities are isolated by running a simulation in which membrane parameters are kept constant. For example, from the fitting of Amar et al. [10] it is seen that going from 22°C to 40°C, the pore radius increased by 1.72% while the membrane thickness decreased by 53% with respect to solute transport and ~4% with respect to water transport (cf. Fig 17 in reference [10]). Over this temperature range, the diffusivities of the sodium and chloride ions increased by ~55% each while the solvent viscosity reduced by ~30%. In the simulation, when variation of pore radius and membrane thickness are accounted for in addition to that of the solvent and ion mobilities, the decrease in rejection of sodium-chloride going from 22°C to 40°C is ~50% (cf. Fig. 5). On the other hand, in the simulation, in order to isolate the effect of solvent and ion mobilities, if the membrane structural parameters are kept constant at the values corresponding to 22°C, and only solvent viscosity and ion diffusivity are varied corresponding to the temperature increase from 22°C to 40°C, the ion rejection reduces by only ~5%. Figure 5 shows that the change in membrane volumetric charge value from -200mol/m^3 to -50mol/m^3 (decrease by 75%), when all other parameters (pore radius, effective thickness, solvent viscosity and ion diffusivity) are kept constant corresponding to values at 22°C, the membrane volumetric charge density by itself reduces the rejection ratio by almost four fold. These numbers clearly illustrate that the variation of the membrane parameters causes a larger percentage change in rejection ratio (and hence ion transport) than the solvent viscosity and the ion diffusivity combined.

4.2.3. Change in the three modes of solute transport: convection, diffusion and electromigration with temperature

When temperature increases, the higher solvent flux carries greater amount of solute with it, causing the increased solute convection (cf. Fig. 5). The overall term $K_{i,c}C_{i,pore}J_w$ is therefore larger for each solute at higher temperatures. Furthermore, at higher temperature, the increase in solute diffusivity causes the

diffusive transport to increase. Regarding diffusive transport, a reduction in rejection ratio due to the increase in temperature implies that the concentration gradient across the membrane is also reduced since there is a smaller fall of concentration across the membrane, thereby causing the $\frac{dC_{i,pore}}{dx}$ term in the Nernst-Planck equation to be reduced in steady state. However, the increase in solute diffusivity due to increase in temperature over-compensates for this effect and overall, the diffusive term $-D_{i,pore} \frac{dC_{i,pore}}{dx}$ is greater in magnitude at higher temperature. Similar to the concentration gradient, the potential gradient across the membrane is smaller in magnitude at higher temperature. However, the electromigrative flux increases at higher temperature predominantly due to the effect of increased solute diffusivity.

4.2.4. Effect of membrane charge on chloride ion transport

From Fig. 5c, showing the magnitudes of the different modes of transport of the chloride ion within the membrane at various negative values of membrane charge, we see that the diffusion is the dominant mode of transport and it becomes larger at larger magnitudes of membrane charge. This is because the negative chloride ion is repelled by the negatively charged membrane and so its concentration within the membrane $C_{Cl^-,pore}$ is small, leading the convective and electromigrative fluxes to be small, and they reduce further at a greater magnitude of negative membrane charge. The chloride ion must have equal solute transport through the membrane as the sodium ion, however, in order to maintain electroneutrality and so the reduced convective and electromigrative fluxes are compensated for by the diffusive flux, which therefore becomes the dominant mode of transport for the chloride ion. At greater magnitudes of negative membrane charge, the intra-membrane concentration for the chloride ion reduces further and hence diffusion becomes increasingly dominant (Fig. 5c). Along a similar line of reasoning, for positive values of membrane charge (Fig. 6), the chloride ions are attracted into the membrane, causing its intra-membrane concentration to be large compared to that within negatively charged membranes. Thus, in membranes with a positive charge, chloride transport is predominantly convective and electromigrative (Fig. 6c). For a positively charged membrane (Fig. 6), the membrane potential is positive and decreases in magnitude across the membrane from feed to permeate side. The electromigration of the negatively

charged chloride ions is in the direction towards the more positive membrane potential (from permeate to feed side), opposite to the overall solute transport. The solute transport and rejection of sodium and chloride ions when the membrane is positively charged is given in Fig. 6.

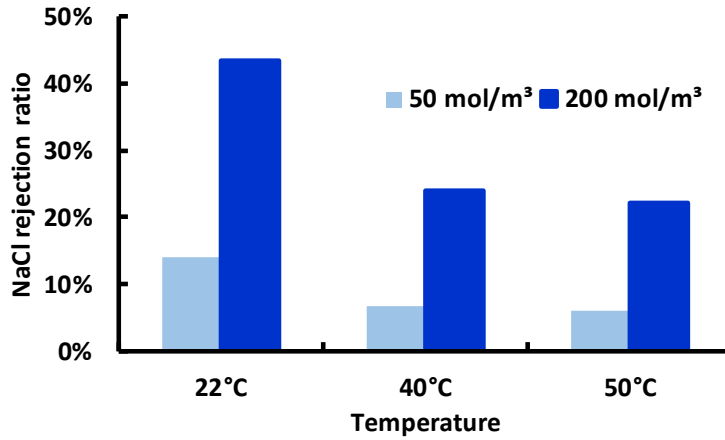


Fig. 6a. NaCl rejection ratio vs. T

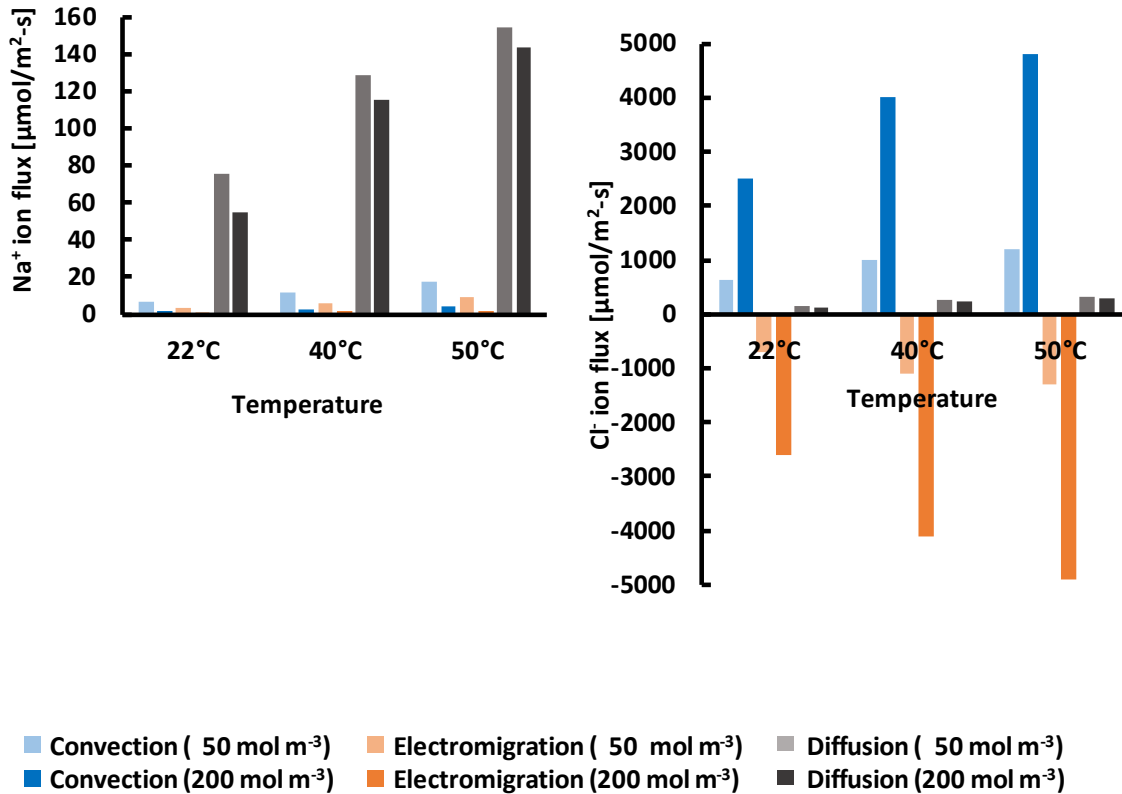


Fig. 6b. Na⁺ flux vs. T

Fig. 6c. Cl⁻ flux vs. T

Figure 6. For a positively charged NF membrane (50 or 200 mol m⁻³), modeling results for rejection and solute transport of Na⁺ and Cl⁻ ions in a 0.01 M NaCl solution at different temperatures: (a) rejection of NaCl; (b) transport of Na⁺ ions by the three modes; and (c) transport of Cl⁻ ions by the three modes.

4.2.5. Sodium ion transport

For sodium ions, for each value of membrane charge at each temperature, the convective flux is always greater in magnitude than the electromigrative i.e. opposite to the behavior of chloride ions flux (Fig. 5 and Fig. 6). The reason is that the ratio of convective to electromigrative flux $R_{i,C/E}$ is greater for sodium than for chloride, where $R_{i,C/E}$ is defined as:

$$R_{i,C/E} = \frac{\text{Convection}_i}{\text{Electromigration}_i} = \frac{K_{i,c}J_w\Delta xRT}{z_iD_{i,pore}\Delta\psi F} \quad (6)$$

where $\Delta\psi$ is the potential drop across the section of the membrane under consideration (or the entire thickness of the membrane if the potential profile is linear) and is equal for all ions in the system. Thus the ratio of magnitudes of $R_{Cl^-,C/E}$ to $R_{Na^+,C/E}$ is given by:

$$\frac{\left| R_{Cl^-,C/E} \right|}{\left| R_{Na^+,C/E} \right|} = \frac{K_{Cl^-,c} D_{Na^+,pore}}{K_{Na^+,c} D_{Cl^-,pore}} \quad (7)$$

This ratio is less than unity, and therefore convection is dominant over electromigration for sodium ions while it is the opposite for chloride ions.

4.2.6. Summary and implications of NaCl transport at higher temperature

1. Solvent and net solute transport increase with increase in temperature.
2. All of the individual modes of solute transport, i.e. convection, diffusion and electromigration, increase in magnitude with temperature.
3. The cumulative effect of changes in membrane properties with temperature is more dominant in influencing solute transport than the combined effect of the corresponding changes in solvent viscosity and ion diffusivity with temperature.

4. The convective mode of solute transport increases in magnitude with temperature predominantly due to the increase in solvent transport. The diffusive and electromigrative modes of transport increase in magnitude with temperature predominantly due to increase in solute diffusivity with temperature.
5. In negatively charged membranes, anion transport is predominantly diffusive while cation transport is predominantly convective. The situation is reversed for positively charged membranes.

4.3. Magnesium-chloride (MgCl_2) transport as a function of temperature

This section considers magnesium-chloride, following a similar path to that for sodium-chloride in the previous section. Mg^{2+} rejection is desirable for scale control in common thermal desalination processes, and in several aspects, Mg^{2+} rejection is representative of other divalent ions. However, from the current section and from section 4.5., it is clear that rejection of this ion is highly dependent on the feed composition. In this study, the concentration of magnesium-chloride salt is taken as 5 mol/m^3 (0.005 M) so that the feed solution contains 10 mol/m^3 (0.01 M) of chloride ions. Thus the concentration of chloride ions in the study of sodium-chloride and magnesium-chloride are equal.

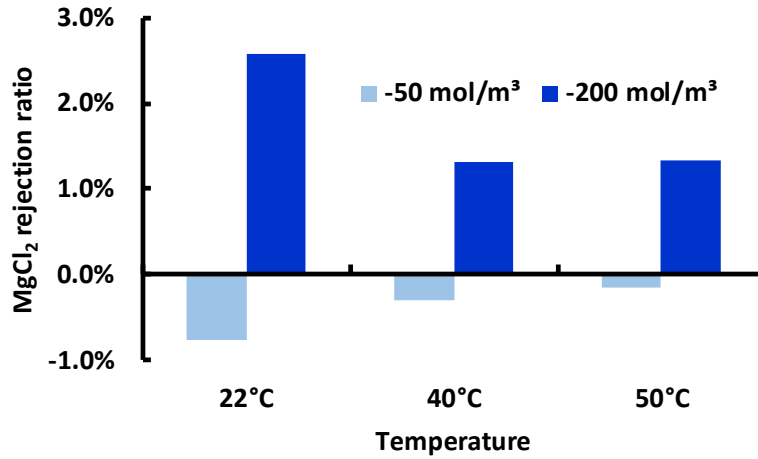
4.3.1. Change in solution and membrane properties with temperature

As mentioned in section 4.2., simulation results are provided only at temperatures for which Amar et al. [10] provide structural parameter values. Again, similar to the case of sodium-chloride, in going from 22°C to 40°C , the diffusivities of both ions increased by $\sim 55\%$, and the fitting parameters of Amar et al. show an increase of pore radius by 1.72% and decrease in membrane thickness by $\sim 53\%$ with respect to solute transport and $\sim 4\%$ with respect to water transport. The simulations show that the combined effect of the change of solvent viscosity and ion diffusivity play a relatively small role in explaining the change in ion rejection (and hence transport) for the given change in temperature compared to the combined effect of the membrane structural parameters. Similar to the approach in section 4.2., the effects of these

two sets of parameters (solute and solvent mobilities versus membrane structural parameters) can be separated by running the simulation in two stages. At first, all effects are varied with temperature together and subsequently another simulation is done in which membrane parameters are kept constant. To that end, in the simulation, if the pore radius and membrane thickness are kept at values corresponding to 22°C and only the solvent viscosity and ion diffusivity values are changed to those at 40°C, the ion rejection increases by 5.3% and 0.1% respectively for a membrane charge of -50 mol/m^3 and 50 mol/m^3 , going from 22°C to 40°C. However, when all parameters in the simulation (pore radius, effective thickness, solvent viscosity and ion diffusivity) are allowed to change to values corresponding to 40°C, the rejection ratio of the ions decreases by ~60% and 3% for these cases. The effect of reducing the negative value of membrane charge from -200 mol/m^3 to -50 mol/m^3 independently at 22°C reduces the rejection ratio by 129%.

4.3.2. Comparison of MgCl_2 and NaCl transport in negative and positively charged membranes

The larger charge on multivalent ions, and in most cases, their larger Stokes radii and lower diffusivities compared to monovalent ions cause significant differences in the rejection performance by NF. This aspect is of crucial importance for membrane design at higher temperatures, as in many cases, such as seawater desalination, it is desirable to reject mainly the divalent ions. Solute transport by the different modes and rejection ratio for the Mg^{2+} and Cl^- ions at different temperatures for membranes with negative and positive charges are shown in Fig. 7 and Fig. 8 respectively.



7a. MgCl₂ rejection ratio flux vs. T

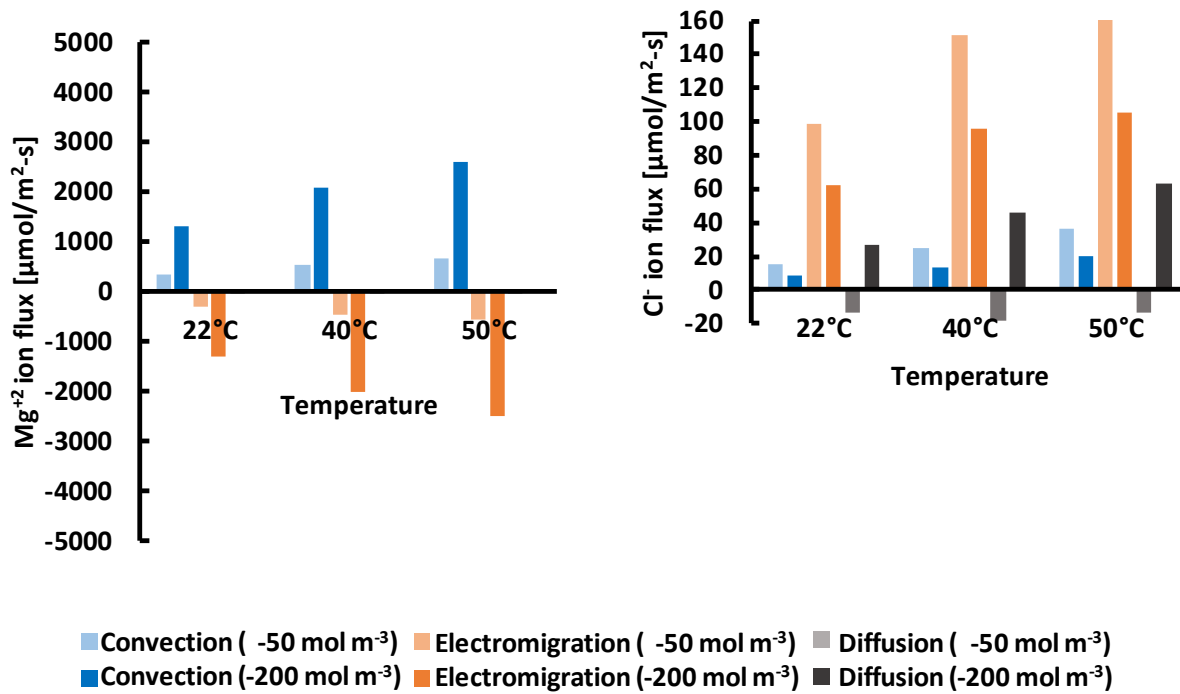


Fig. 7b. Mg²⁺ flux vs. T

Fig. 7c. Cl⁻ flux vs. T

Figure 7. For a negatively charged NF membrane (-50 or -200 mol m^{-3}), modeling results of rejection and solute transport of Mg^{2+} and Cl^{-} ions in a $0.005M$ $MgCl_2$ solution at different temperatures: (a) rejection of $MgCl_2$; (b) transport of Mg^{2+} ions by the three modes; and (c) transport of Cl^{-} ions by the three modes.

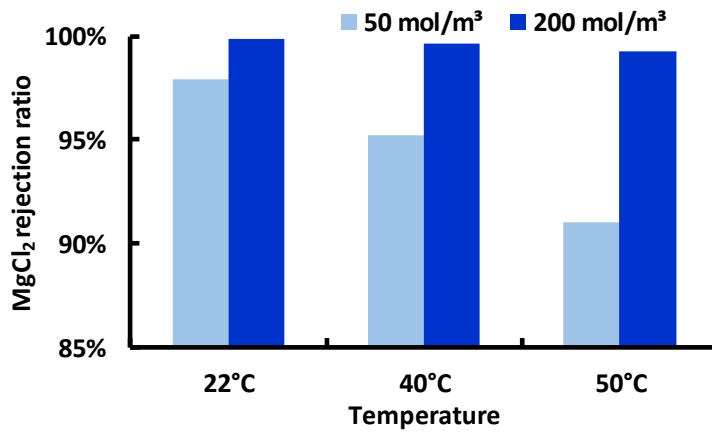
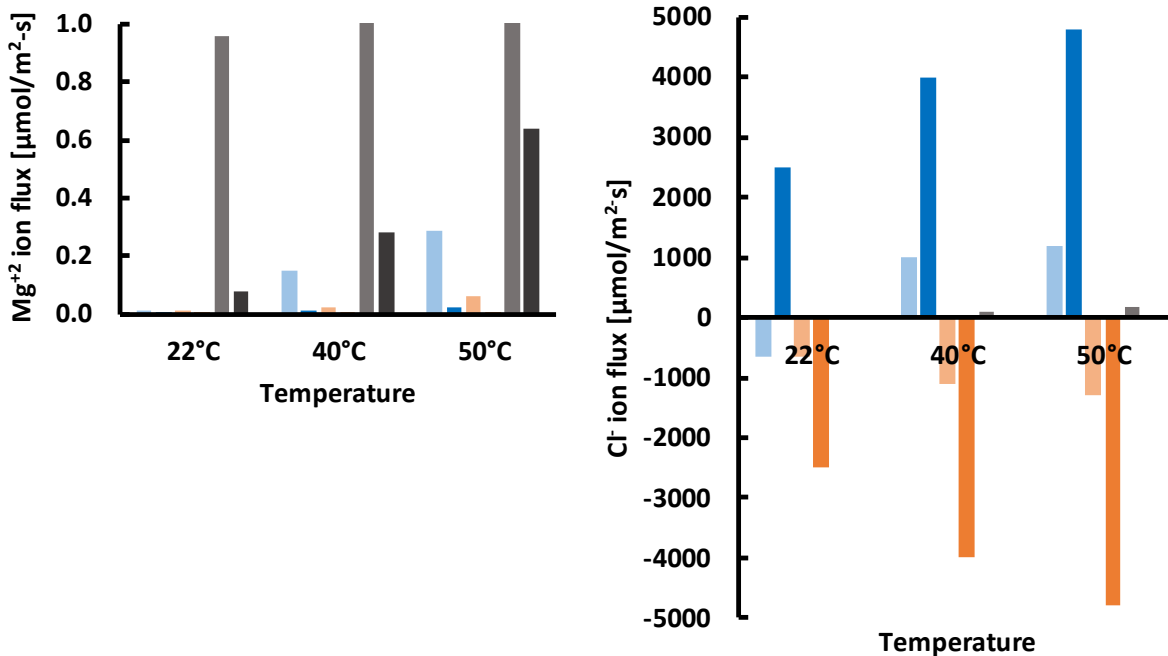


Fig. 8b. MgCl₂ rejection ratio vs. T



■ Convection (50 mol m⁻³)
 ■ Electromigration (50 mol m⁻³)
 ■ Diffusion (50 mol m⁻³)
■ Convection (200 mol m⁻³)
 ■ Electromigration (200 mol m⁻³)
 ■ Diffusion (200 mol m⁻³)

Fig. 8b. Mg²⁺ flux vs. T

Fig. 8c. Cl⁻ flux vs. T

Figure 8. For a positively charged NF membrane (50 or 200 mol m⁻³), modeling results of rejection and solute transport of Mg²⁺ and Cl⁻ ions in a 0.005M MgCl₂ solution at different temperatures and positive membrane charges: (a) rejection of MgCl₂; (b) transport of Mg²⁺ ions by the three modes; and (c) transport of Cl⁻ ions by the three modes.

The trends observed for the magnesium ion for different values of membrane charge (Fig. 7 and Fig. 8) are very similar to those observed for the sodium ion (Fig. 5 and Fig. 6). For both magnesium-chloride and sodium-chloride, salt rejection is higher for a positive membrane charge compared to a negative membrane with equal magnitude of charge, due to steric exclusion. Since both cations are larger than the chloride ion, they experience a high steric exclusion, resulting to reduced movement of itself and its counter-ion into a positive membrane. One exception to the similarities between the salts is that for the chloride ion, as seen from Fig. 7c, when negatively charged membranes are considered, electromigration is dominant over diffusion for the magnesium-chloride solution (while for sodium-chloride solution, diffusion was greater in magnitude than electromigration for the chloride ion). This can be explained by looking at the ratio $R_{i, E/D}$:

$$R_{i, E/D} = \frac{\text{Electromigration}_i}{\text{Diffusion}_i} = \left(\frac{C_{i,pore} \Delta\psi}{\Delta C_{i,pore}} \right) \left(\frac{z_i F}{RT} \right) \quad (8)$$

Here $\Delta C_{i,pore}$ is the concentration drop across the section of the membrane under consideration, or the entire thickness of the membrane if the concentration profile is linear. The ratio $\left| R_{Cl^-, E/D} \right|$ is greater than one in the magnesium-chloride solution while it is smaller than one for sodium-chloride in a negatively charged membrane, which explains why one mode of transport is dominant over the other for the two salts considered. This can be further explained by observing the non-constant terms $C_{i,pore}$, $\Delta\psi$ and $\Delta C_{i,pore}$ in Eq. (8) for the magnesium-chloride and sodium-chloride solutions, as discussed presently. For the chloride ion, at any given value of negative membrane charge, the mean concentration within the membrane $C_{i,pore}$ and potential drop across the membrane $\Delta\psi$ are higher for the magnesium-chloride solution compared to the sodium-chloride solution. On the other hand, the concentration drop across the membrane $\Delta C_{i,pore}$ is lower for the magnesium-chloride solution compared to the sodium-chloride solution. The reason for the higher intra-membrane concentration of chloride ions in the case of

magnesium-chloride compared to sodium-chloride is due to the higher valence of magnesium compared to sodium, thereby drawing more chloride into the membrane to maintain intra-membrane electro-neutrality. Although the number of equivalents (i.e. number of units of charge provided by the ion) of Na^+ and Mg^{2+} inside the membrane are approximately equal (and equal to the membrane volumetric charge density), the concentration of the ion of higher valence is marginally higher (and increases as the valence of the ion increases, even if the feed concentration of the Cl^- is kept same overall all cases to ensure a fair comparison). Since the Cl^- has a lower concentration in the membrane (it has the same charge as the membrane and is electrically repelled by it), even a small difference in the number of equivalents of Na^+ and Mg^{2+} in the membrane causes a large difference in the number of equivalents of Cl^- present. For example, considering the NaCl solution, for a membrane of -200 mol/m^3 charge at 50°C , the mean intramembrane concentration of Na^+ is 200.2 mol/m^3 and that of Cl^- is thus 0.2 mol/m^3 . In comparison, for the MgCl_2 case, the intramembrane concentration of Mg^{2+} is 100.4 mol/m^3 (i.e., 200.8 equivalents of Mg^{2+} per m^3), and the Cl^- concentration is 0.8 mol/m^3 (four times as large as the NaCl case). Thus, a difference of only 0.3% in the number of equivalents of Mg^{2+} compared to Na^+ resulted in the Cl^- concentration to be four times in the MgCl_2 case compared to the NaCl case. As mentioned above, the concentration drop of Cl^- across the membrane $\Delta C_{i,pore}$ is lower for the magnesium-chloride solution compared to the sodium-chloride solution. This is explained by the lower rejection ratio in the magnesium-chloride case, leading to a smaller drop of concentration from feed to permeate side. The potential drop across the membrane is higher in magnesium-chloride since the magnesium ion is larger: in negatively charged membranes, electromigration counteracts convective transport thus limiting accumulation of positive charges in the permeate solution [20]. Consequently, a larger ion requires a higher potential gradient to drive it back through the membrane to the feed side. Thus, the preceding comparison between the respective $C_{i,pore}$, $\Delta\psi$ and $\Delta C_{i,pore}$ terms of Cl^- in the magnesium-chloride case and the sodium-chloride case explains why the ratio $R_{\text{Cl}^-, E/D}$ is larger than one in the former case and smaller than 1 in the latter case. This discussion thus explains the reason for the exception to the

similarities between trends observed for magnesium-chloride and sodium chloride; that for the chloride ion, in a negatively charged membrane electromigration is dominant over diffusion in the magnesium-chloride solution.

4.3.3 Negative rejection of MgCl_2

For a membrane with -50 mol/m^3 charge, the magnesium-chloride solution shows a negative rejection ratio (Fig. 7a), meaning that, in steady state, the concentration of the salt is higher on the permeate side than the feed side. This also results in the diffusive flux of both ions to be in the negative direction, from permeate to feed, opposite to the overall solute flux (diffusion always takes place from the region of higher concentration to lower concentration). The rejection ratio becomes positive as soon as the charge is slightly increased or decreased (by about 40 mol/m^3). The rejection ratio is negative at -50 mol/m^3 because the membrane offers adequate attractive force to the magnesium ions, while not allowing the repulsion towards the chloride ions to dominate. On the other hand, making the membrane more positive offers increased repulsion towards the magnesium ions. Even at zero membrane charge, a small positive rejection of magnesium-chloride is observed, since the ions still experience steric exclusion and there is no help from the membrane charge to draw the ions in. At -50 mol/m^3 membrane charge, the rejection ratio is negative for all three temperatures, and the rejection ratio of magnesium-chloride increases (becomes less negative) with increasing temperature, in contrast to all other cases studied. This increase in rejection ratio with increase in temperature occurs because the permeate-side partitioning effect (Eq. 3) for the dominant intra-membrane ion, Mg^{2+} , increases with temperature and hence the drop in concentration from within the membrane to the permeate solution becomes sharper. Despite the increase in rejection ratio with temperature, the net solute transport of magnesium-chloride increases with temperature due to the increasing water flux, thereby increasing the convective salt flux. The mean intramembrane concentration of both ions also increase with increase in temperature.

4.3.4. Summary and implications of MgCl₂ transport at higher temperature

1. Similar to the case of NaCl in section 4.2., the dominant influence on solute transport with increasing temperature was the cumulative temperature-induced changes in membrane properties, while only a small impact was made by temperature-induced changes in solvent viscosity and solute diffusivity combined.
2. Similar trends were observed for the Mg²⁺ and Na⁺ ions (c.f. section 4.2.) for the impact of temperature and membrane charge density on solute transport modes and ion rejection.
3. For both NaCl and MgCl₂, the salt rejection is higher for a positively charged membrane of a given magnitude, compared to a negatively charged membrane of equal magnitude.
4. In a negatively charged membrane, the intramembrane concentration of Cl⁻ is higher for the MgCl₂ case compared to the NaCl case because the Mg²⁺ ion (which has a higher valence than the Na⁺) pulls in more chloride ions. In general, a cation of higher valence has a marginally higher intramembrane concentration for a given fixed (negative) membrane charge value, but this has a magnified effect on the anion concentration, and the anion intramembrane concentration increases significantly for cations of larger valence. For a fair comparison in this discussion, as the valence of the cation is increased, the chloride ion concentration in solution is kept equal for all salts by reducing the net salt concentration. For example, 0.01M NaCl and 0.005M MgCl₂ have the same molar concentrations of Cl⁻ ions in solution.
5. It is possible to obtain a negative rejection ratio of MgCl₂ for a certain value of negative membrane charge density, such that the rejection ratio increases (becomes less negative) with increase in temperature.

4.4. Effect of dielectric exclusion on solute transport

In nanofiltration, dielectric exclusion is an important mode of solute exclusion, along with steric and charge-based exclusion. In the previous sections of this work, the effect of dielectric exclusion was not

considered, since our approach is to examine the impact of membrane parameters individually. In the model used for this work, dielectric exclusion governed only by the Born effect is considered, which accounts for the solvation energy barrier for the ion to enter the pore, resulting in a decreased dielectric constant of the solvent within the pore [14] [21] [24]. Thus, the Born effect accounts for the energy penalty for an ion to shed its hydration shell when moving from a fully solvated state in bulk solution to the constricted passage within the pore, where there isn't enough 'space' for all of the ion's hydration shells. Dielectric exclusion works to reject ions irrespective of their charge, unlike the charge-based exclusion (wherein the charged membrane attracts counter-ions while repelling co-ions).

4.4.1. Variation of pore dielectric constant with temperature

According to Bowen et al. [21], the expression for dielectric constant within the membrane pores can be given by the expression in Eq. 9 which assumes that the solvent, i.e. water molecules, occur in a thin annulus lining the inner pore periphery and the enclosed region has bulk dielectric properties.

$$\varepsilon_{pore}(T) = 80 - 2(80 - \varepsilon^*(T)) \left(\frac{d}{r_{pore}(T)} \right) + (80 - \varepsilon^*(T)) \left(\frac{d}{r_{pore}(T)} \right)^2 \quad (9)$$

In Eq. 9, ε_{pore} is the effective dielectric constant of water within the pore, ε^* is the dielectric constant of the annulus of water covering the inner wall of the pore, r_{pore} is the pore radius and d is the thickness of one water molecule. The above expression gives the temperature-dependent pore dielectric constant as a function of the temperature-dependent pore radius and dielectric constant of the annulus of water lining the pore inner surface. According to Bowen et al. [21], the dielectric constant of the ordered layer of water forming the annulus, ε^* was found to be 31 from their experiments at 25°C. Since the extensive experimentation to determine the exact variation of this quantity as a function of temperature is beyond the scope of the current work, the dielectric constant of the oriented water molecules is assumed to change

similarly to that of bulk water over the given temperature range and thus to decrease by 10.87% from 22°C to 50°C [43]. Equation 9 is thus used to estimate the pore dielectric constant at 50°C, by using fitted values of pore radius from Amar et al. [10], assuming the size of the water molecule does not change with temperature. According to this calculation, the intra-pore dielectric constant at 50°C is found to be 45.37. Using the same approach, the pore dielectric constant is 44.11 at 22°C. Although Roy et al. [14] use a pore dielectric constant of 56.5 for the Desal5DK membrane to match the results for seawater desalination in the SWCC Umm Lujj plant at 25°C, Eq. 9 provides a different value. Without further efforts on experimental determination of the pore dielectric constant, it is not possible to arrive at a more conclusive value of pore dielectric constant; furthermore, the value may also depend on the feed composition [44] [45]. Bowen et al. [21] used a sodium-chloride solution to obtain their value for the dielectric constant of the ordered water layer (ϵ^*) used in Eq. 9.

4.4.2. Sensitivity of NaCl rejection to pore dielectric constant

In this section, the impact of the pore dielectric constant on solute transport will be illustrated. For instance, the simulation results show that in going from a pore dielectric constant value of 80.4 to 45 (decrease by ~44%), the solute transport of sodium-chloride at 50°C at membrane charges of 0, -50 mol/m³ and -200 mol/m³ reduced by about 6%, 56% and 82% respectively. The value of pore dielectric constant to compare against, 80.4, was chosen because it is the bulk dielectric constant of water and hence when the pore dielectric constant is set equal to this value, the Born solvation energy barrier is zero, effectively removing the effect of dielectric exclusion [20]. As stated in section 4.4.1., the pore dielectric constant of the Desal5DK membrane at 50°C was estimated to be around 45. The above percentage changes in net solute transport due to pore dielectric constant at fixed values of membrane charge give an indication that dielectric constant is an important factor to consider in explaining the change in rejection ratio of ions with temperature.

4.4.3. Effect of dielectric exclusion on solute transport modes and rejection

Due to dielectric exclusion, the convective and electromigrative modes of transport for the chloride ion are significantly reduced, since the dielectric exclusion allows less chloride ions to enter the membrane. Therefore, the intra-membrane concentration $C_{Cl^-,pore}$ is reduced. The intra-pore concentration of the sodium ion has to remain almost unchanged in order to satisfy electroneutrality and so the electromigrative and convective terms for the sodium ion remain practically unaffected by dielectric exclusion in a negative membrane. Although the rejection ratio is higher due to dielectric exclusion, the concentration gradient across the membrane thickness $\frac{dC_{i,pore}}{dx}$ (and hence diffusive transport) is less compared to when dielectric exclusion is not considered for both Na^+ and Cl^- ions. For a given feed concentration, a higher rejection usually implies a higher concentration gradient through the membrane because of the smaller permeate-side concentration. Conversely, a higher concentration gradient usually signifies a higher rejection ratio. However, due to dielectric exclusion, the net solute transport for both ions is drastically reduced due to the Born exclusion effect and the higher rejection is reflected in a large partitioning effect on the permeate side (cf. Eq. 3); hence there is a steeper fall in concentration between a point just within the membrane (on the permeate side) and the permeate concentration.

4.4.4. Summary and implications of dielectric exclusion on NF solute transport

1. Increased dielectric exclusion (caused by reduced magnitude of pore dielectric constant) causes the rejection of all ions to increase.
2. Increased dielectric exclusion causes increased partitioning effect at the membrane-solution interfaces and reduced solute transport through the membrane.

4.5. Seawater nanofiltration at different temperatures

In this section, the solute transport and rejection ratio for each ion in seawater is analyzed at two different temperatures. This analysis is pertinent to NF as a pretreatment for thermal desalination systems, in which the feed water temperature may vary over the course of the day or over the year. All membrane

parameters (both structural and electrical) were used for the analysis. The minimum and maximum temperatures used in the study thus far (22°C and 50°C) were considered, in order to clearly discern the effect of temperature. The concentrations of the ions in seawater are taken from Table 2 from Roy et al. [14]. The values of the membrane structural parameters and dielectric constant as obtained previously for the Desal5DK membrane at 22°C and 50°C (cf. Table 2) are used to simulate the nanofiltration of seawater at these temperatures. In order to simplify the analysis and since the membrane charge of the Desal5DK membrane at different temperatures for seawater feed composition are not known at present, the membrane charge will be kept fixed at -80 mol/m^3 (the value fitted by Roy et al. in [14]). Thus, the present analysis provides insight into the changes in seawater nanofiltration due to the change in membrane structural parameters and pore dielectric constant with temperature. Although the exact fitted values of membrane charge for this feed at both of the two temperatures considered would be desirable for the analysis, the dielectric exclusion effect evaluated using the pore dielectric constants mentioned in section 4.4.1 (44.11 and 45.37 respectively for 22°C and 50°C) is significant and is in fact the dominant mode of exclusion (over steric and Donnan exclusion) at both temperatures. For the analysis, one spiral-wound membrane element will be simulated using the model developed by Roy et al. [14] and the variation of water recovery ratio and rejection ratio with temperature will be observed in addition to the solute transport of each ion.

Table 2. The following table summarizes the membrane parameters used at 22°C and 50°C:

Parameter	<u>Pore radius</u>	<u>Effective active layer thickness</u>		<u>Membrane volumetric charge density</u>	<u>Pore dielectric constant</u>
	r_{pore} [nm]	$\frac{\Delta x}{A_k}$ [μm]		C_X [mol/m^3]	ϵ_{pore}
Value at 22°C	0.58	from solute	from water	-80	44.11
Value at 50°C	0.67	0.56	2.67	-80	45.37

Source	Amar et al. [10]	Amar et al. [10]	Roy et al. [14] (assumed constant for this analysis)	Calculation using Eq. 9
--------	------------------	------------------	------------------------------------------------------------	----------------------------

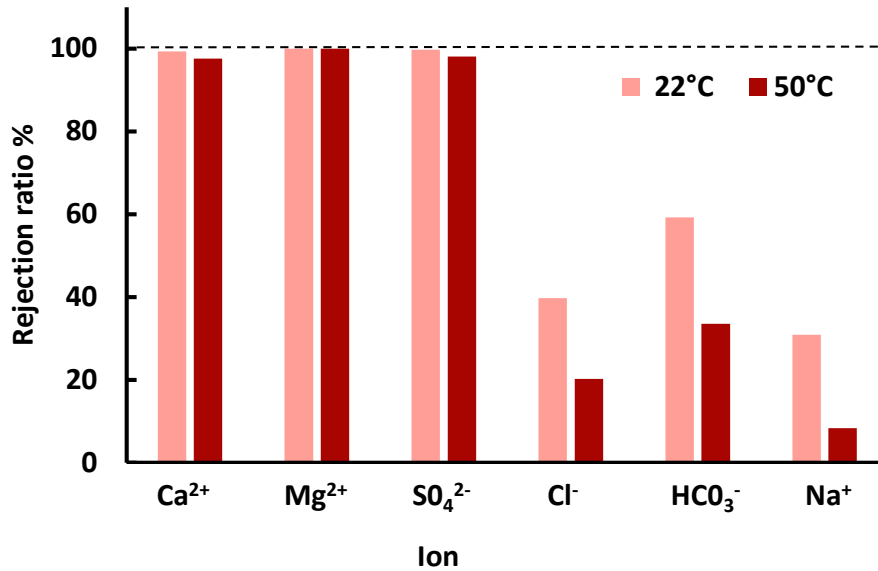


Figure 9. Rejection ratios of the primary ionic constituents of seawater at 22°C and 50°C as obtained from modeling a single element of a spiral-wound module at those temperatures.

Figure 9 shows that the rejection ratios of the divalent ions calcium, magnesium and sulfate are almost 100% at both temperatures, although the rejection ratio decreases slightly at the higher temperature. The monovalent ions are rejected to a much lesser extent and the maximum rejection among them is observed for the bicarbonate ion.

Figure 10 shows the solute transport by each mode for each ion at the two temperatures considered. In Fig. 10, the diffusion values for the Na⁺ and Cl⁻ ions at 50°C (dark grey) are not shown entirely since they are too large. In this figure, the value shown is ~7000 μmol/m²-s at 50°C for both ions, but in fact they go up to ~15700 μmol/m²-s and ~16700 μmol/m²-s respectively. Results for seawater ions other than Na⁺ and Cl⁻ are shown in the supplementary information to focus on the non-dominant ions.

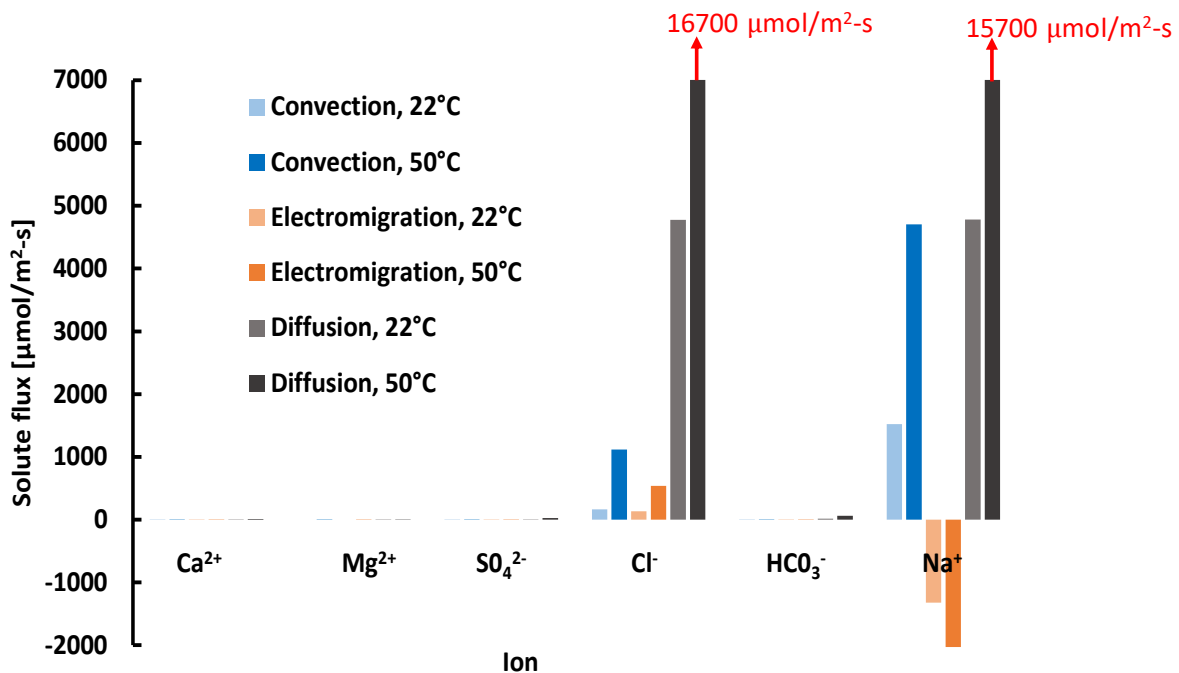


Figure 10. Flux of ions in seawater through a negatively-charged (-80 mol m^{-3}) NF membrane, by the three different modes (convection, electromigration, and diffusion) at 22°C and 50°C. Conditions were obtained from modeling a single element of a spiral-wound module at those temperatures. The diffusion values for the Na⁺ and Cl⁻ ions at 50°C (dark grey) are not shown entirely since they are too large. In this figure, the value shown is $\sim 7000 \text{ } \mu\text{mol/m}^2\text{-s}$ at 50°C for both ions, but in fact they go up to $\sim 15700 \text{ } \mu\text{mol/m}^2\text{-s}$ and $\sim 16700 \text{ } \mu\text{mol/m}^2\text{-s}$ respectively. Results for seawater ions other than Na⁺ and Cl⁻ are shown in the supplementary information to focus on the non-dominant ions.

4.5.1. Effect of feed concentration and membrane exclusion modes on seawater ions

Considering a seawater feed, the net solute transport for each of the divalent ions and bicarbonate is a few orders of magnitude less than that of the chloride and sodium ions (Fig. 10). This is partly due to the fact that the feed concentration of the sodium and chloride ions are much higher than that of the other ions in seawater; and partly due to the much larger exclusion experienced by the divalent ions, mainly in the form of dielectric exclusion. The dielectric exclusion is highest for the magnesium ion, followed by the calcium ion, the sulfate ion and then the monovalent ions. The negative charge on the membrane is predominantly neutralized by the sodium ions, since it has the highest intra-membrane concentration. Although this is slightly surprising, considering the negatively charged membrane attracts the positive divalent ions most

strongly into the membrane, it can be explained by the fact that the dielectric exclusion is higher for the two divalent cations and this effect dominates that of the charge-based attraction. Furthermore, the feed concentration of calcium and magnesium are much lower than that of the sodium ion, thereby reducing the amount of these ions 'available' to enter the membrane. The two monovalent anions chloride and bicarbonate experience similar magnitudes of steric, dielectric and Donnan exclusion, however the intra-membrane concentration of the bicarbonate is much lower than that of the chloride due to its smaller feed concentration and hence lesser 'availability'. Unsurprisingly, the divalent anion sulfate experiences the largest amount of charge-based exclusion and also has high steric and dielectric exclusion causing high rejection. The above arguments explain why the intra-membrane concentration in the descending order is sodium, chloride, bicarbonate, sulfate, calcium and magnesium. In seawater, the convective mode is more dominant than the electromigrative mode for the sodium and chloride ions, as shown in Fig. 10. This dominance of convection occurs because the membrane potential for the seawater case is sufficiently low to bring the weight of the electromigrative term down.

4.5.2. Percentage change in rejection of individual ions with temperature

In regard to seawater feed, the net solute transport of the divalent ions is a few orders of magnitude less than that of the monovalent ions at both temperatures. However, the increase in net solute transport from 22°C to 50°C is higher for the divalent ions (10-30 fold) than the monovalent ions (3-5 fold). For the divalent ions, the mode of transport that increases the most sharply is the diffusive mode, while for the monovalent ions, it is the convective mode. The exception to this trend is Na^+ , for which diffusion increases marginally greater than convection. Such a sharp increase in the diffusive mode for the divalent ions is attributed to the sharp increase in the intra-membrane concentration on the feed side (just within the membrane), for the temperature rise from 22°C to 50°C due to the sharp change in the partitioning effects. This increase in concentration within the membrane facing the feed side results in a larger concentration gradient within the membrane and thus increased diffusion. The percentage change of the rejection ratio of the divalent ions with increase in temperature is lower than that of the monovalent ions,

however, partly because their numerical values are larger. Overall, for the membrane studied and the given feed composition, the rejection ratio of the calcium ion shows the greater sensitivity to temperature (higher percentage decrease in rejection ratio with increase in temperature) between the two divalent cations. The sodium ion rejection has the largest percentage decrease in rejection ratio with increase in temperature among monovalents, and the chloride and bicarbonate rejections show almost equal percentage change in rejection ratio for the temperature change. Finally, the recovery ratio for the single element was seen to increase from 8.3% at 22°C to 23.9% at 50°C.

4.5.3. Summary and implications for seawater transport at higher temperature

1. Rejection ratio of all divalent ions is ~100% at both temperatures studied, although it reduces slightly at the higher temperature. The rejection ratios of the monovalent ions are significantly less than that of the divalent ions at both temperatures and reduce notably with increase in temperature.
2. Solute transport of each ion through the membrane depends on its feed concentration. Regarding each of the divalent ions and the bicarbonate ion, their feed concentrations are significantly lower than that of sodium and chloride ions in seawater. This factor contributes to their net solute transport being a few orders of magnitude less than that of the sodium and chloride ions.
3. Each of the divalent ions experience large exclusion by the membrane, predominantly in the form of dielectric exclusion, resulting to their lower transport through the membrane relative to sodium and chloride ions. In fact, the sodium and chloride ions have the greatest intramembrane concentration. Even though the negatively charged membrane attracts the divalent cations more strongly, their entry is restricted by exclusion effects.
4. The percentage increase in net solute transport with temperature is significantly higher for the divalent ions compared to the monovalent ions. This trend in solute transport among the ions in seawater is due to the reduction in the exclusion mechanisms at the higher temperature, which affects the divalent ions more strongly.

5. The percentage decrease in rejection ratio with increase in temperature is lower for the divalent ions compared to the monovalent ions.
6. As a result of the change in membrane parameters and the decrease in solvent viscosity, overall membrane water flux increases substantially at higher temperatures. For a spiral-wound element operating on Arabian Gulf seawater, the water recovery increases from 8.3% at 22°C to 23.9% at 50°C as per the modeling analysis.

4.6. Summary of temperature effects

A summary of how the important model parameters and results change with temperature is provided in the following table. For this analysis, only one parameter is changed at a time and a positive rejection ratio regime, as seen in most cases described in the paper, is assumed.

Expression	Variable	Change at higher temperature	Impact on membrane performance
ν	Solvent kinematic viscosity	Decreases	Increase in solvent flux, which by itself increases rejection ratio. However as per Stokes-Einstein Eq. (ref. [27]) a decrease in viscosity increases ion diffusivity, which lowers rejection ratio.
r_{pore}	Pore radius	Increases (c.f. ref [10])	Increase in solvent flux Reduction in steric hindrance of solutes.
$(\Delta x / A_k)_{solute}$	Effective membrane thickness (from solute)	Varies (c.f. ref [10])	A reduction in this parameter causes reduced rejection ratio

$(\Delta x / A_k)_{water}$	Effective membrane thickness (from water)	Varies (c.f. ref [10])	A reduction in this parameter causes increased solvent flux
D_i	Solute diffusivity	Increases	Reduced rejection ratio
ϵ_{pore}	Pore dielectric constant	Increases	Increase in this parameter causes reduced dielectric exclusion and hence reduced rejection ratio
$-D_{i,pore} \frac{dC_{i,pore}}{dx}$	Diffusive transport	Generally decreases, increases (becomes less negative) when ion rejection is in negative regime Increases in magnitude	
$K_{i,c} C_{i,pore} J_w$	Convective transport	Increases in magnitude	
$-\frac{z_i C_{i,pore} D_{i,pore}}{RT} F \frac{d\psi}{dx}$	Electromigrative transport	Increases in magnitude	
Φ_i	Steric exclusion	Decreases due to pore expansion	
Φ_B	Dielectric exclusion	Decreases due to increase in pore dielectric constant	
$exp\left(-\frac{z_i F}{RT} \psi_D\right)\Big _{interface}$	Donnan partitioning	Reduces for membrane counter-ion, increases for membrane co-ion	

5. Conclusions and outlook

To the authors' knowledge, the present work is the first to examine the impact of temperature on nanofiltration, examining the mechanisms of solute transport and exclusion in different feed solutions at different temperatures. The DSPM-DE model is used in which solute transport is described by the Nernst-Planck equation within the membrane, thereby capturing three different modes of solute transport: the convective, diffusive, and electromigrative modes. The DSPM-DE model involves three exclusion mechanisms governing entry of solute into the membrane: the steric, dielectric, and Donnan exclusion mechanisms. Each of these modes of transport and exclusion for individual ions vary with temperature, thereby affecting how a given membrane rejects ions differently at different temperatures. Ions differ from one-another in terms of size, valence, and diffusivity and these factors, coupled with changes in the membrane itself due to temperature determine which ions show greater change of rejection with temperature change.

Apart from those mentioned in the section summaries/implications, the following conclusions are obtained from this study:

1. Electroneutrality within the membrane is the key driving factor in determining how much of each ion enters the membrane at a given value of water flux. When several ions of like charge are present, the exclusion mechanisms are the deciding factor for competition among the different ions and determine which ions are 'preferred' to enter the membrane.
2. In the analysis of seawater ions, one major effect causing large rejection of scale-causing divalent ions (Mg^{2+} , Ca^{2+} , SO_4^{2-}) is the large dielectric exclusion experienced by these ions. Thus, lower ϵ_{pore} causing greater dielectric exclusion is beneficial for NF membranes aiming to remove these scalants.
3. In light of the preceding discussions, for higher temperature applications, membranes with lower temperature-dependent structural changes are desirable. Specifically, membranes whose pore

radius increases less are preferred not only because they can maintain high steric exclusion, but also low intra-pore dielectric constant (cf. Eq. 9) resulting in high dielectric exclusion. Regarding membrane charge, the desired value depends on the ions to be rejected. For membranes attempting to remove Mg^{2+} and Ca^{2+} , an increased negative charge with temperature is disadvantageous. A higher negative membrane charge will aid rejection of the SO_4^{2-} ions, however.

Experimental work to accurately fit the membrane charge and pore dielectric constant as a function of temperature is desirable in future, although the present analysis provides clear insight into the nature of changes in solute transport and rejection that occur as a result of temperature change.

6. Acknowledgements

The authors would like to thank King Fahd University of Petroleum and Minerals for funding the research reported in this paper through the Center for Clean Water and Clean Energy at MIT and KFUPM. The authors would also like to thank Margaret Bertoni for assistance with graphics.

References

- [1] D. M. Warsinger, E. W. Tow, K. G. Nayar, L. A. Maswadeh and J.H. Lienhard V "Energy efficiency of batch and semi-batch (CCRO) reverse osmosis desalination.," *Water Research*, vol. 106, pp. 272-282., 2016.
- [2] A. Mohammad, Y. Teow, W. Ang, Y. Chung, D. Oatley-Radcliffe and N. Hilal, "Nanofiltration membranes review: Recent advances and future prospects," *Desalination*, vol. 356, pp. 226-254, 2015.
- [3] W. R. Bowen and J. S. Welfoot, "Modelling of membrane nanofiltration—pore size distribution effects," *Chemical Engineering Science*, p. 1393–1407, 2002.
- [4] N. Hilal, H. Al-Zoubi, N. A. Darwish, A. W. Mohammad and M. Abu Arabi, "A comprehensive review of nanofiltration membranes: Treatment, pretreatment, modelling, and atomic force microscopy," *Desalination*, vol. 170, no. 3, pp. 281-308, 2004.

- [5] W. R. Bowen, B. Cassey, P. Jones and D. L. Oatley, "Modelling the performance of membrane nanofiltration—application to an industrially relevant separation," *Journal of Membrane Science*, vol. 242, no. 1, pp. 211-220., 2004.
- [6] D. L. Oatley, B. Cassey, P. Jones and W. R. Bowen, "Modelling the performance of membrane nanofiltration—recovery of a high-value product from a process waste stream," *Chemical Engineering Science*, vol. 60, no. 7, pp. 1953-1964, 2005.
- [7] P. Eriksson, "Nanofiltration extends the range of membrane filtration," *Environmental Progress*, vol. 7, no. 1, p. 58–62, 1988.
- [8] R. Rautenbach and A. Gröschl, "Separation potential of nanofiltration membranes," *Desalination*, vol. 77, pp. 73-84, 1990.
- [9] D.M. Warsinger, K.H. Mistry, K.G. Nayar, H.W. Chung and J.H. Lienhard V, "Entropy generation of desalination powered by variable temperature waste heat," *Entropy*, vol. 17, no. 11, pp. 7530-7566, 2015.
- [10] N. B. Amar, H. Saidani, A. Deratani and J. Palmeri, "Effect of Temperature on the Transport of Water and Neutral Solutes across Nanofiltration Membranes," *Langmuir*, vol. 23, pp. 2937-2952, 2007.
- [11] M. Manttari, A. Pihlajamaki, E. Kaipainen and M. Nystrom, "Effect of temperature and membrane pre-treatment by pressure on the filtration properties of nanofiltration membranes," *Desalination*, vol. 145, pp. 81-86, 2002.
- [12] M. J. H. Snow, D. de Winter, R. Buckingham, J. Campbell and J. Wagner, "New techniques for extreme conditions: high temperature reverse osmosis and nanofiltration," *Desalination*, vol. 105, pp. 57-61, 1996.
- [13] M. K. M. Al-Sofi, A. Hassan, G. Mustafa and A. Dalvi, "Nanofiltration as a means of achieving higher TBT of ≥ 120 °C in MSF," *Desalination*, vol. 118, p. 123–129, 1998.
- [14] Y. Roy, M. H. Sharqawy and J. H. Lienhard V, "Modeling of flat-sheet and spiral-wound nanofiltration configurations and its application in seawater nanofiltration," *Journal of Membrane Science*, vol. 493, pp. 360-372, 2015.
- [15] O. Labban, C. Liu, T. Chong and J. H. Lienhard V, "Fundamentals of low-pressure nanofiltration: Membrane characterization, modeling, and understanding the multi-ionic interactions in water softening," *Journal of Membrane Science*, vol. 521, pp. 18-32, 2017.
- [16] M. A. M. Muthumareeswaran and G. Agarwal, "Ultrafiltration membrane for effective removal of chromium ions from potable water.," *Scientific Reports 7*, 2017.

- [17] S. Levchenko and V. Freger, "Breaking the Symmetry: Mitigating Scaling in Tertiary Treatment of Waste Effluents Using a Positively Charged Nanofiltration Membrane," *Environmental Science & Technology Letters*, vol. 3, no. 9, pp. 339-343, 2016.
- [18] A. Kowalik-Klimczak, M. Zalewski and P. Gierycz, "Prediction of the chromium (III) separation from acidic salt solutions on nanofiltration membranes using donnan and steric partitioning pore (DSP) model," *Architecture Civil Engineering Environment*, vol. 9, no. 3, pp. 135-140, 2016.
- [19] S. Blumenschein, A. Böcking, U. Kätzel, S. Postel and M. Wessling, " Rejection modeling of ceramic membranes in organic solvent nanofiltration," *Journal of Membrane Science*, vol. 510, pp. 191-200, 2016.
- [20] V. Geraldés and A. M. B. Alves, "Computer program for simulation of mass transport in nanofiltration membranes," *Journal of Membrane Science*, vol. 321, no. 2, p. 172–182, 2008.
- [21] W. R. Bowen and J. S. Welfoot, "Modelling the performance of membrane nanofiltration—critical assessment and model development," *Chemical Engineering Science*, vol. 57, no. 7, p. 1121–1137, 2002.
- [22] S. Bandini and D. Vezzani, "Nanofiltration modeling: the role of dielectric exclusion in membrane characterization," *Chemical Engineering Science*, vol. 58, no. 15, p. 3303–3326, 2003.
- [23] W. R. Bowen and A. W. Mohammad, "Characterization and prediction of nanofiltration membrane performance a general assessment," *Trans IChemE*, vol. 76, pp. 885-893, 1996.
- [24] D. L. Oatley, L. Llenas, R. Pérez, P. M. Williams, X. Martínez-Lladó and M. Rovira, "Review of the dielectric properties of nanofiltration membranes and verification of the single oriented layer approximation," *Advances in Colloid and Interface Science*, vol. 173, p. 1–11, 2012.
- [25] N. S. Kotrapannavar, A. A. Hussain, M. E. E. Abashar, I. S. Al-Mutaz, T. M. Aminabhavi and M. N. Nadagouda, "Prediction of physical properties of nanofiltration membranes for neutral and charged solutes," *Desalination*, vol. 280, no. 1-3, p. 174–182, 2011.
- [26] J. Schaep, B. Van der Bruggen, S. Uytterhoeven, R. Croux, C. Vandecasteele, D. Wilms, E. Van Houtte and F. Vanlerberghe, "Removal of hardness from groundwater by nanofiltration," *Desalination*, vol. 119, pp. 295-302, 1998.
- [27] M. Nilsson, G. Tragardh and K. Ostergren, "The influence of pH, salt and temperature on nanofiltration performance," *Journal of Membrane Science*, vol. 312, pp. 97-106, 2008.
- [28] W. R. Bowen and A. W. Mohammad, "Diafiltration by nanofiltration: prediction and optimization.," *AIChE Journal*, vol. 44, no. 8, pp. 1799-1812, 1998.

- [29] J. L. Anderson and D. M. Malone, "Mechanism of osmotic flow in porous membranes," *Biophysical Journal*, vol. 14, no. 12, p. 957, 1974.
- [30] J. L. Anderson and J. A. Quinn, "Restricted transport in small pores: a model for steric exclusion and hindered particle motion," *Biophysical Journal*, vol. 14, no. 2, p. 130, 1974.
- [31] X.-L. Wang, T. T. Tsuru, S. Nakao and S. Kimura, "Evaluation of pore structure and electrical properties of nanofiltration membranes," *Journal of Chemical Engineering of Japan*, vol. 28, no. 2, pp. 186-192, 1995.
- [32] X.-L. Wang, T. T. Tsuru, S. Nakao and S. Kimura, "Electrolyte transport through nanofiltration membranes by the space-charge model and the comparison with Teorell-Meyer-Sievers model," *Journal of Membrane Science*, vol. 103, no. 1, pp. 117-133, 1995.
- [33] D. Vezzani and S. Bandini, "Donnan equilibrium and dielectric exclusion for characterization of nanofiltration membranes," *Desalination*, vol. 149, no. 1, pp. 477-483, 2002.
- [34] M. Higa, A. Kira, A. Tanioka and K. Miyasaka, "Ionic partition equilibrium in a charged membrane immersed in a mixed ionic solution," *Journal of the Chemical Society, Faraday Transactions*, vol. 89, no. 18, pp. 3433-3435, 1993.
- [35] R. Renou, A. Ghoufi, A. Szymczyk, H. Zhu, J. Neyt and P. Malfreyt, "Nanoconfined electrolyte solutions in porous hydrophilic silica membranes," *The Journal of Physical Chemistry C*, vol. 117, no. 21, pp. 11017-11027, 2013.
- [36] O. Beckstein, K. Tai and M. Sansom, "Not ions alone: barriers to ion permeation in nanopores and channels," *Journal of the American Chemical Society*, vol. 126, no. 45, pp. 14694-14695, 2004.
- [37] A. Yaroshchuk, "Non-steric mechanisms of nanofiltration: superposition of Donnan and dielectric exclusion," *Separation and Purification Technology*, vol. 22, pp. 143-158, 2001.
- [38] M. G. Davidson and W. M. Deen, "Hydrodynamic theory for the hindered transport of flexible macromolecules in porous membranes," *Journal of Membrane Science*, vol. 35, no. 2, pp. 167-192, 1988.
- [39] P. Dechadilok and W. Deen, "Hindrance factors for diffusion and convection in pores," *Industrial and Engineering Chemistry Research*, vol. 45, no. 21, pp. 6953-6959, 2006.
- [40] G. M. Mavrovouniotis and H. Brenner, "Hindered sedimentation diffusion and dispersion coefficients for Brownian spheres in circular cylindrical pores," *Journal of Colloid and Interface Science*, vol. 124, no. 1, pp. 269-283, 1988.
- [41] J. Ennis, H. Zhang, G. Stevens, J. Perera, P. Scales and S. Carnie, "Mobility of protein through a

porous membrane," *Journal of Membrane Science*, vol. 119, no. 1, pp. 47-58, 1996.

- [42] M. L. Huber, R. A. Perkins, A. Laesecke, D. G. Friend, J. V. Sengers, M. J. Assael, I. N. Metaxa, E. Vogel, R. Mareš and K. Miyagawa, "New international formulation for the viscosity of H₂O," *Journal of Physical and Chemical Reference Data*, vol. 38, no. 2, pp. 101-125, 2009.
- [43] G. Akerlof, "Dielectric constants of some organic solvent-water mixtures at various temperatures," *The Journal of the American Chemical Society*, vol. 54, no. 11, pp. 4125-4139, 1932.
- [44] H. L. Friedman, "Theory of the dielectric constant of solutions," *The Journal of Chemical Physics*, vol. 76, no. 2, pp. 1092-1105, 1982.
- [45] J. B. Hubbard, P. Colonomos and P. G. Wolynes, "Molecular theory of solvated ion dynamics. III. The kinetic dielectric decrement.," *The Journal of Chemical Physics*, vol. 76, no. 1, pp. 2652-2661, 1979.

Appendix A.

Membrane structural parameters at different temperatures from the fitting by Amar et al. [10]:

Parameter	r_{pore} [nm]	$\Delta x / A_k$ [μm]	$\Delta x / A_k$ [μm]
		(solute)	(water)
22°C	0.58	0.98	2.20
40°C	0.59	0.46	2.11
50°C	0.67	0.56	2.67

Supplementary Information, Roy et al., 2017

The results below show solute transport of sodium-chloride and magnesium-chloride at 30°C together with those presented in the original paper (22°C, 40°C and 50°C). The inclusion of results at this temperature illustrates that the discussions presented in the paper hold through the entire temperature range 22- 50°C. Subsequently, solute transport of various seawater ions other than Na⁺ and Cl⁻ are shown to magnify the results for the non-dominant ions.

S.1. Plots for NaCl at 22°C, 30°C, 40°C and 50°C.

S.1.1. Negative membrane charge:

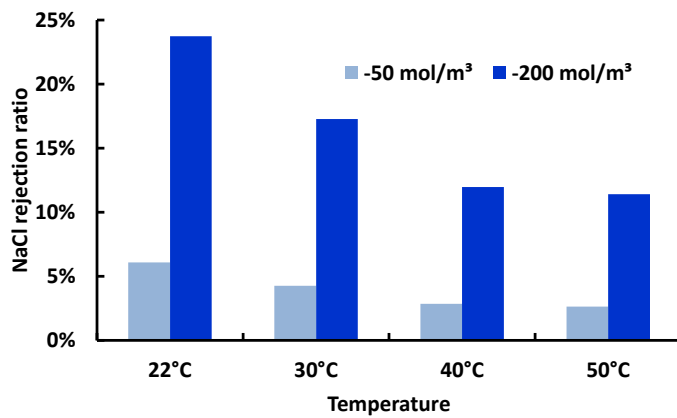


Fig. S.1.1a. NaCl rejection ratio vs. T

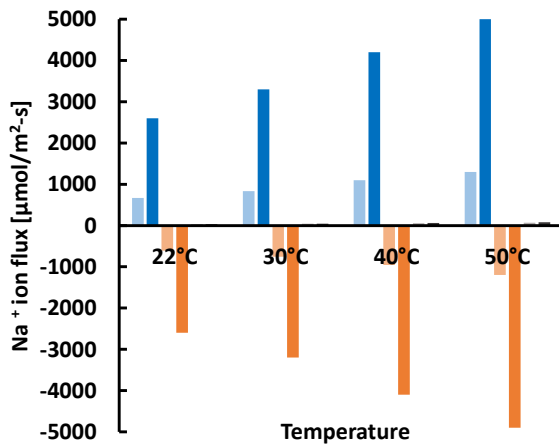


Fig. S.1.1b. Na⁺ flux vs. T

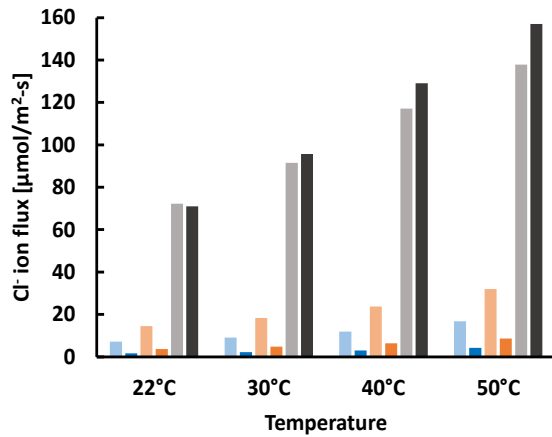


Fig. S.1.1c. Cl⁻ flux vs. T

- Convection (-50 mol m⁻³) ■ Electromigration (-50 mol m⁻³) ■ Diffusion (-50 mol m⁻³)
- Convection (-200 mol m⁻³) ■ Electromigration (-200 mol m⁻³) ■ Diffusion (-200 mol m⁻³)

Figure S.1. For a negatively charged NF membrane (-50 or -200 mol m^{-3}), modeling results for rejection and solute transport of Na^+ and Cl^- ions in a 0.01M NaCl solution at 4 different temperatures, 22°C, 30°C, 40°C and 50°C: (a) rejection of NaCl; (b) transport of Na^+ ions by the three modes; and (c) transport of Cl^- ions by the three modes.

S.1.2. Positive membrane charge:

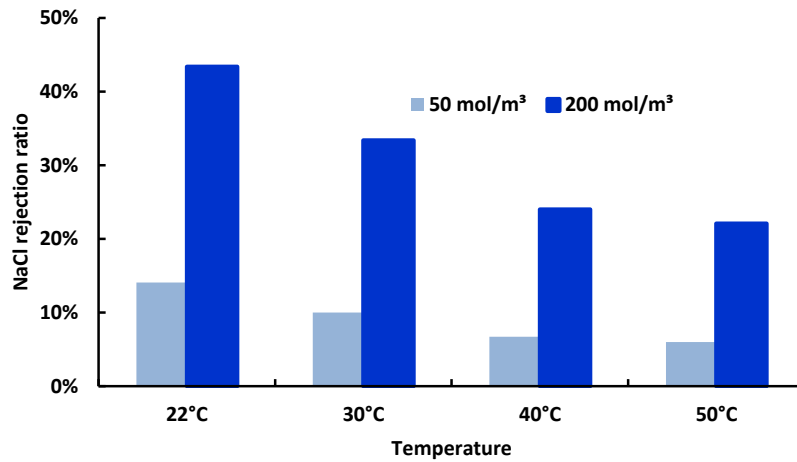


Fig. S.1.2a. NaCl rejection ratio vs. T

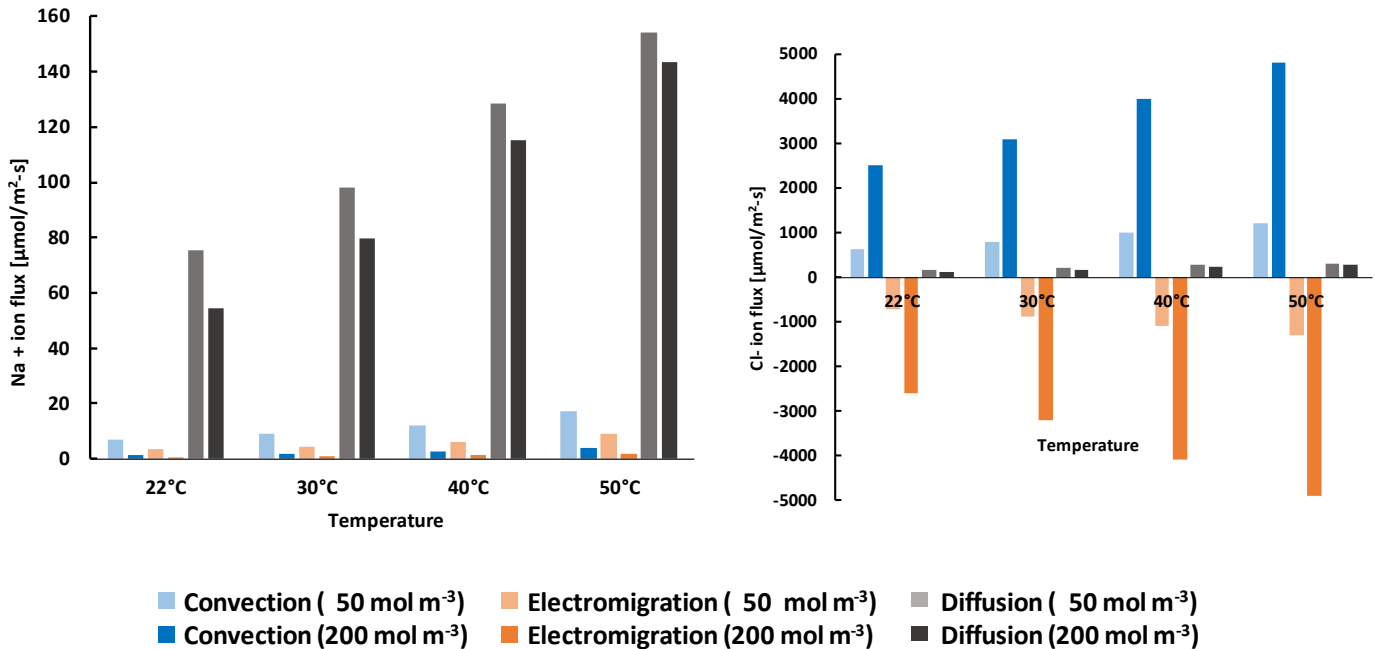


Fig. S.1.2b. Na⁺ flux vs. T

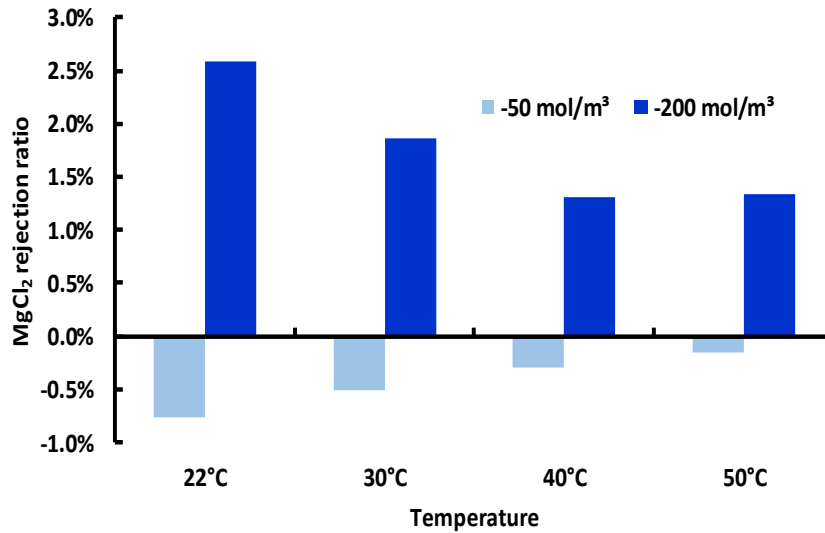
Fig. S.1.2c. Cl⁻ flux vs. T

Figure S.2. For a positively charged NF membrane ($+50$ or $+200$ mol m^{-3}), modeling results for rejection and solute transport of Na^+ and Cl^- ions in a 0.01M NaCl solution at 4 different temperatures, at 22°C,

30°C, 40°C and 50°C: (a) rejection of NaCl; (b) transport of Na⁺ ions by the three modes; and (c) transport of Cl⁻ ions by the three modes.

S.2. Plots for MgCl₂ at 22°C, 30°C, 40°C and 50°C.

S.2.1. Negative membrane charge:



S.2.1a. MgCl₂ rejection ratio flux vs. T

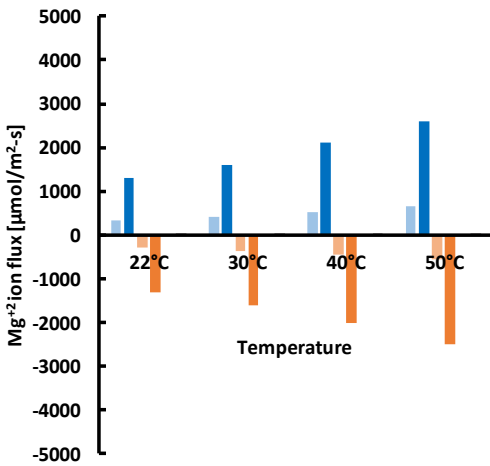


Fig. S.2.1b. Mg²⁺ flux vs. T

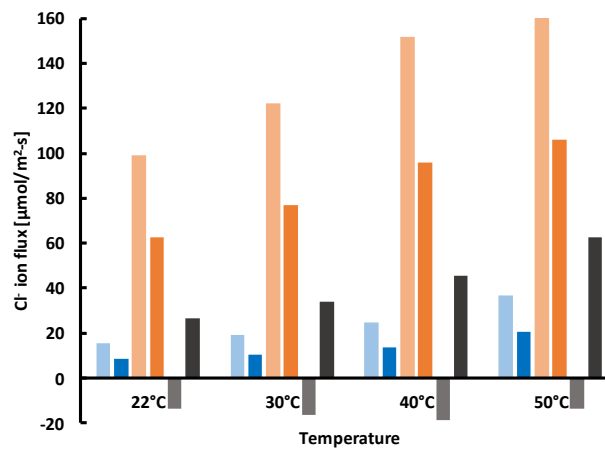
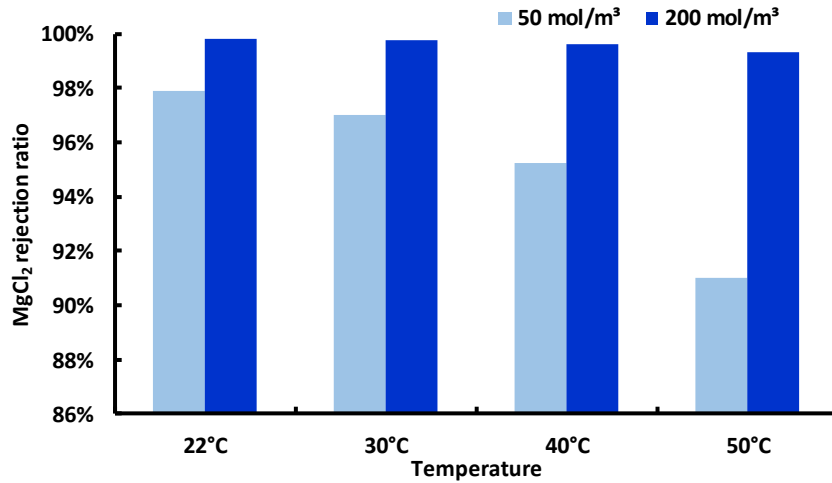


Fig. S.2.1c. Cl⁻ flux vs. T

- Convection (-50 mol m⁻³) ■ Electromigration (-50 mol m⁻³) ■ Diffusion (-50 mol m⁻³)
- Convection (-200 mol m⁻³) ■ Electromigration (-200 mol m⁻³) ■ Diffusion (-200 mol m⁻³)

Figure S.2.1. For a negatively charged NF membrane (-50 or -200 mol m^{-3}), modeling results of rejection and solute transport of Mg^{2+} and Cl^{-} ions in a $0.005M$ $MgCl_2$ solution at 4 different temperatures, $22^{\circ}C$, $30^{\circ}C$, $40^{\circ}C$ and $50^{\circ}C$: (a) rejection of $MgCl_2$; (b) transport of Mg^{2+} ions by the three modes; and (c) transport of Cl^{-} ions by the three modes.

S.2.2. Positive membrane charge:



S.2.2a. $MgCl_2$ rejection ratio flux vs. T

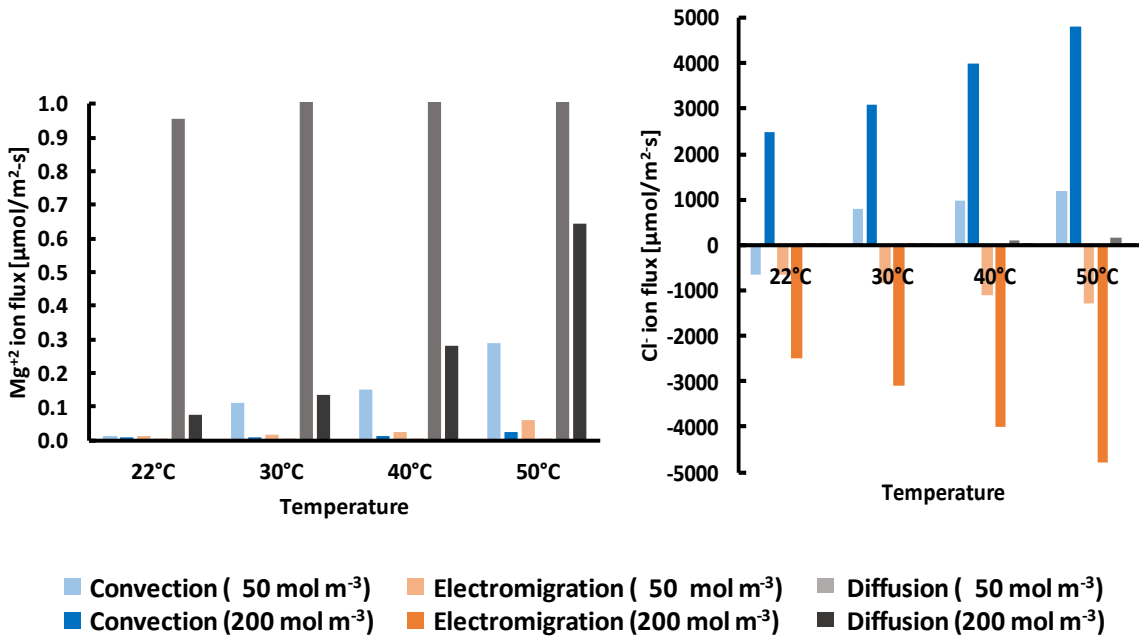


Fig. S.2.2b. Mg^{2+} flux vs. T

Fig. S.2.2c. Cl^{-} flux vs. T

Figure S.2.2. For a positively charged NF membrane (+50 or +200 mol m⁻³), modeling results of rejection and solute transport of Mg²⁺ and Cl⁻ ions in a 0.005M MgCl₂ solution at 4 different temperatures, 22°C, 30°C, 40°C and 50°C: (a) rejection of MgCl₂; (b) transport of Mg²⁺ ions by the three modes; and (c) transport of Cl⁻ ions by the three modes.

S.3. Solute transport modes of various seawater ions other than Na⁺ and Cl⁻.

